UC Irvine

Title

Features of turbulence during wildland fires in forested and grassland environments

Permalink

https://escholarship.org/uc/item/8m60f6vw

Authors

Desai, Ajinkya

Heilman, Warren E

Skowronski, Nicholas S

et al.

Publication Date

2023-07-01

DOI

10.1016/j.agrformet.2023.109501

Copyright Information

Peer reviewed
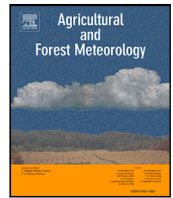
Features of turbulence during wildland fires in forested and grassland environments

Ajinkya Desai [a],[*],[1], Warren E. Heilman [b],[2], Nicholas S. Skowronski [c],[3], Kenneth L. Clark [d],[4], Michael R. Gallagher [d],[5], Craig B. Clements [e],[6], Tirtha Banerjee [a],[7]

[a] *Department of Civil and Environmental Engineering, University of California, Irvine, CA 92697, USA*
[b] *Northern Research Station, USDA Forest Service, Lansing, MI 48910, USA*
[c] *Northern Research Station, USDA Forest Service, Morgantown, WV 26505, USA*
[d] *Northern Research Station, USDA Forest Service, New Lisbon, NJ 08064, USA*
[e] *Department of Meteorology and Climate Science, San José State University, San José, CA, USA*

ARTICLE INFO

ABSTRACT

Fire-induced turbulence and the feedback into the fire, following ambient changes, differ for forested (sub-canopy) and grassland environments. Here, we synthesize observations from multiple experimental surface fires: two sub-canopy backing fires, one sub-canopy heading fire, and a grassland heading fire. We identify and compare the most essential coherent structures and processes of each case from the turbulent momentum fluxes and turbulent kinetic energy (TKE) budget terms. In the sub-canopy burns, turbulent eddies are strongest near the canopy top: high streamwise turbulent flux accompanies low cross-stream turbulent flux and vice versa. In the grassland fire, both streamwise and cross-stream eddies strengthen simultaneously until a certain height, informing a vertical length scale for the fire-influence. Moreover, the forward sweep from streamwise eddies assists in the fire spread by pushing hot gases towards unburnt fuel. In the sub-canopy fires, shear production and buoyancy production are more substantial near the canopy top for more intense fires, while their magnitudes decrease with decreasing fire intensity. At mid-canopy-height scales, buoyancy production dominates shear production, becoming the key mechanism for vertical transport of TKE. In the grassland fire, shear production dominates buoyancy production near the surface and is insignificant beyond a certain height relative to the flame length, while buoyancy production increases with height, becoming substantial further away from the surface. Turbulent transport terms are also active in both environments. For intense sub-canopy fires, there is a loss in TKE due to its expulsion to the boundary layer aloft via the transport term, compensated by a reversal process: TKE influx via the transport term. In the grassland fire, the transport term mimics this behavior until a certain height. The insights into the relative significance of the respective turbulent fluxes and TKE budget terms in each environment can help simplify the complex system of equations governing fire physics.

1. Introduction

Fire-induced turbulence has considerable impact on scalar dispersion and momentum transport both during and after the passage of the fire-front across the fuel in wildland fire environments. The dispersion of scalars such as smoke in turn affects visibility and human health, especially for residents in the wildland-urban interface, while the transport of firebrands (embers) poses a severe risk of spotting up to several kilometers away from the fire-front (Thurston et al., 2017). Moreover, fire behavior is closely linked with the ambient turbulence

---

* Corresponding author.
  E-mail address: ajinkyad@uci.edu (A. Desai).
[1] 0000-0001-5642-4193
[2] 0000-0003-4217-5100
[3] 0000-0002-5801-5614
[4] 0000-0003-0534-9677
[5] 0000-0003-0175-558X
[6] 0000-0001-9999-8621
[7] 0000-0002-5153-9474

(canopy turbulence in the forested environments). Depending on the environment, turbulence in the canopy or the atmospheric boundary layer demonstrably affects fire spread-rates (Sun et al., 2009; Banerjee, 2020), occasionally in unexpected ways. With a deep necessity to understand fire-induced turbulence both in grassland and forested environments, fire simulations (Linn et al., 2002; Morvan et al., 2006; Mell et al., 2007; Mueller et al., 2014) as well as *in-situ* measurements from burns on small as well as management scales (Desai et al., 2022; Seto et al., 2013; Heilman et al., 2013, 2015, 2017, 2021a,b) have gained importance. However, the excessive computational overhead involved in simulating fires in forested and grassland environments (Colman and Linn, 2007; Zhou et al., 2007) make them less amenable for extended use. While a fast-running simulation platform like QUIC-fire (Linn et al., 2020) is able to circumvent this issue, its wind solver (QUIC-URB) outputs the time-averaged flow field, which makes it difficult to analyze the turbulence-driving fire behavior. Given these constraints on computational models, careful examination of observed data from burn experiments can be useful in investigating the coherent motions that characterize fire-induced turbulence. Such examination can potentially also allow for the simplification of the governing equations describing fire behavior based on the relative importance of the different terms involved. In the past, empirically derived models (Finney, 1998, 2006; Andrews, 2014) based on the widely used model by Rothermel (1972) have been successful in simplifying the complex set of governing (thermal, chemistry, fluid flow) equations for successful operational use via the parameterization of several physical quantities. However, these models are based on laboratory experiments so that their application on management scales is limited. Another limitation is their inability to provide insights into the complex turbulent environment arising from fire-atmosphere interaction.

Despite their usefulness in understanding the physics underlying fire-induced turbulence, studies relying on experimental data have only recently gathered momentum because of the high risk of damage posed to equipment during data collection in the presence of a flame (Clements et al., 2007). Here, we review the key findings of some of the few leading empirical studies that attempted to untangle the complex dynamics underlying fire-atmosphere interaction. Recent studies by Heilman et al. (2015, 2019) explored turbulent kinetic energy (TKE) levels at different heights of a 20 m measurement tower, the energy spectrum of the velocity components, and patterns in the turbulent heat and momentum fluxes for two different backing surface fires in the New Jersey Pinelands National Reserve (forested environment), one of high intensity in 2011 and the other of lower intensity in 2012. For the higher intensity fire, fire-induced TKE near the canopy top was found to be much more substantial compared to the lower heights, making turbulent diffusion of smoke near the canopy top more important than mixing at lower heights within the canopy. Analysis of 1 minute averaged turbulent momentum fluxes showed that vertical turbulent fluxes contributed 40%–80% to the net momentum flux before, during, and after fire-front-passage (FFP) (Heilman et al., 2019). The relative contribution of the vertical turbulent heat and momentum fluxes to the net heat and momentum fluxes was found to be highest at the mid-canopy height when compared to near the surface or the canopy top. Estimates of the turbulence anisotropy obtained by Heilman et al. (2017) demonstrated the significance of horizontal velocity perturbations over vertical velocity perturbations pre- and post-FFP as well as during FFP periods at all measurement heights. Analysis of the relative contribution of the terms in the TKE budget equations showed that shear production was higher than the buoyancy production at all measurement heights within the overstory vegetation layer pre- and post-FFP. Furthermore, the turbulent transport term resulted in a loss of TKE at all measurement heights during FFP in 2011, while its effect was found to be greatly diminished in the lower-intensity 2012 burn. In a separate study, Heilman et al. (2021b) studied the contribution to turbulent fluxes of sweep-ejection events before, during, and after the passage of a heading (wind-driven) surface fire-front through a

network of 20 m measurement towers during an operational burn in the New Jersey Pine Barrens (under the U.S. Department of Defense–Strategic Environmental Research Program (SERDP)). It was found that pre-FFP and post-FFP periods were characterized by sweeps and ejections, while FFP periods were characterized by sweeps and outward interactions (convection involving the upward flux of wind with high horizontal momentum). These studies encapsulate some of the most recent turbulence analyses on experimental surface fires in forested regions.

The FireFlux experiment was a pioneering study on fire–atmosphere interactions in a grassland fire and set a benchmark for similar studies in the future (Clements et al., 2008). It comprised a heading (wind-driven) experimental grassland fire conducted at the Houston Coastal Center in Texas on 23 February, 2006. Temperature and velocity measurements taken during the experiment by a 43 m instrumented tower were utilized by Clements et al. (2008) for a first-order analysis. Derived quantities such as the velocity spectra, turbulent momentum fluxes, and TKE were analyzed to comment on the turbulence levels induced by the fire-front passage. The turbulence intensity generated by the fire was found to be four to five times greater than the ambient atmospheric turbulence. Furthermore, turbulent fluxes demonstrated a downward transfer of high momentum downstream of the fire-front. Heilman et al. (2021a) took the analysis further with their study of sweep-ejection-like events, which also included results from the three prescribed fires in the New Jersey Pinelands described above. Their focus was on examining how the frequencies of occurrence of sweep-ejection-like events and their contributions to the mean vertical turbulent fluxes of heat and momentum were modulated by the vicinity or presence of the fire. Contrary to conditions in the absence of surface fires, it was found that ejections were completely dominant in their contribution to heat-flux events and outward interaction events substantially overshadowed the contribution of sweeps and ejections to momentum-flux events in both environments. The most frequent events during FFP were heat-flux inward interaction events (flux of warmer air towards the surface) and momentum-flux outward interaction events (explained above) in grassland and forested environments, respectively.

As seen above, previous empirical and semi-empirical studies (Kiefer et al., 2015; Heilman et al., 2017) have taken a keen interest in exploring turbulent fluxes and terms of TKE budget equation pre-, during, and post-FFP for insights into the dominant physical processes characterizing fire-induced turbulence. However, the interpretation of coherent structures inferred from the turbulent fluxes and the TKE budget terms is sensitive to the averaging scheme employed to decompose turbulent signals into the mean and turbulent fluctuations from the mean. Additionally, the effect of the fire on the mean kinetic energy (MKE) budget terms remains to be explored using the existing data. Furthermore, several differences in the fire-turbulence behavior between surface fires in forested and grassland environments remain to be articulated. For instance, we expect the nature of the turbulent transport term to be different, considering that it assumes different levels of importance within the canopy and in the open atmospheric boundary layer in no-fire conditions (Raupach et al., 1996). Heilman et al. (2019) also reflected on the need to understand differences in the behavior of turbulent fluxes for backing and heading fires across all the measurement heights in the canopy. Evidently, there is a need to unify and synthesize observations from burn experiments that have already been conducted via an inter-comparison to develop an over-arching description of the process involved.

The analyses presented by Clements et al. (2007, 2008) and Heilman et al. (2015, 2017, 2019, 2021a,b) for four experimental management-scale burns (one grassland fire; two understory backing fires; one understory heading fire) conducted in Texas in 2006 (FireFlux), in the New Jersey Pinelands National Reserve in 2011 and 2012, and in the New Jersey Pinelands National Reserve in 2019 (SERDP) are synthesized and re-investigated in this study. Here, we aim to fill the

gaps in the previous analyses on these data regarding the coherent motions arising out of fire-atmosphere interaction when juxtaposed with the background canopy (canopy-scale) turbulence or open atmospheric turbulence, depending on the surface-fire environment. High-frequency 10 Hz measurements in the case of the sub-canopy fires and 20 Hz measurements in the case of the grassland fire for velocity and temperature are utilized. We first introduce the data by exploring the slowly-varying parts of the velocity components and temperature for changes occurring in the flow over relatively longer time scales. We then investigate pre-, during, and post- FFP wind-rose statistics for a visual representation of the combined changes induced by the presence of the fire and ambient wind shifts. Finally, we compute the turbulent fluxes and terms of the TKE budget equation; we comment on the effect of the former on the latter and on the physical significance of both. From these quantities, computed at different heights above ground level (AGL), we seek insights into the more persistent coherent structures, the key fire-spread mechanisms, and the dominant turbulence generation and TKE redistribution processes, along with the relevant vertical length scales. Another important and relatively unexplored question of interest is the effect of FFP on the terms of the MKE budget equation, which is investigated here for the sub-canopy surface fires. We aim to draw a comparison of insights among all the three scenarios considered here: heading surface fire beneath the canopy, backing surface fire beneath the canopy, and heading surface fire in a grassland. We set up the analysis in Section 2 and provide a brief background on the data sets in Section 3. In Section 4.1, we compare results from the sub-canopy fires and in Section 4.2, we highlight the attributes that distinguish the grassland fire from the sub-canopy surface fires, thereby synthesizing the key insights from each of the three scenarios considered here. As with most data collected from prescribed burns, the current data were also occasionally influenced by wind variability. We take the opportunity to comment on the effect such variability may have on the fire while simultaneously attempting to summarize the general features that broadly characterize each scenario.

2. Theory

All components of the velocity (u_i in the index notation) and the temperature (T) are decomposed into a relatively slowly-varying component and a fluctuating component: $u_i = \overline{u}_i + u'_i$ and $T = \overline{T} + T'$. Here, the overbar represents time averaging and the quantities marked with prime are the fluctuating terms. The overbar is chosen to represent 1 hour moving averages in the case of the sub-canopy surface fires, while it is chosen to represent 1 minute moving averages in the case of the grassland fire. We represent the streamwise (x), cross-stream (y), and vertical (z) components of velocity at height h by u_h, v_h, and w_h, respectively. We define the streamwise direction (x) as the direction in which the fireline propagates in the case of a heading fire and the direction opposite to fireline propagation in the case of a backing fire. Notwithstanding noticeable variability in the streamwise winds (as expected during a management-scale burn), the wind speeds are the highest in the streamwise direction for the most part, especially at the beginning of each experiment. While the direction of the ambient wind may change (relative to the cardinal directions), both the streamwise and cross-stream directions remain fixed over the course of a burn experiment. Similarly, T_h represents the temperature at height h. No penetration and no-slip conditions at the surface imply that $w_0 = u_0 = v_0 = 0$. Also, h_c denotes the approximated mean canopy height in the case of the sub-canopy surface fires ($h_c = 20$ m).

Next, the TKE budget equation is written as follows (Stull, 2012):

$$\frac{\partial \overline{e}}{\partial t} + \overline{u}_j \frac{\partial \overline{e}}{\partial x_j} = \delta_{i3} \frac{g}{\theta_v} \overline{u'_i \theta'_v} - \overline{u'_i u'_j} \frac{\partial \overline{u}_i}{\partial x_j} - \frac{\partial \overline{u'_j e}}{\partial x_j} - \frac{1}{\rho} \frac{\partial \overline{u'_j p'}}{\partial x_j} - \varepsilon, \quad (1)$$

where e is the TKE, θ_v is the virtual potential temperature of air (approximated here as the moving mean of the temperature, $\overline{T}$), p' is the pressure perturbation, and ε is the TKE dissipation rate. The first,

second, and third terms on the right-hand side are the buoyant production (TKE_{bp}), shear production (TKE_{sp}), and turbulent transport terms (TKE_{tr}), respectively. The fourth term on the right-hand side is the pressure correlation term (not computed in this analysis). Due to the absence of data varying along the streamwise (x) and cross-stream (y) directions for most of the datasets in this study, we cannot compute the following terms: (i) $-\overline{u'w'} \frac{\partial \overline{w}}{\partial x} - \overline{v'w'} \frac{\partial \overline{w}}{\partial y}$ in TKE_{sp} and (ii) $-\frac{\overline{u'e}}{\partial x} - \frac{\overline{v'e}}{\partial y}$ in TKE_{tr}. However, it must be noted that horizontal gradients may be substantial near the fire-fronts. As seen from term (ii), these gradients may drive turbulent transport in the horizontal direction, which can affect fire spread and the interaction between different points along the fire-front (as seen by Desai et al., 2022 in small-scale surface fires). These gradients may also capture the effects arising from horizontal heterogeneity in the fuel (and, thereby, in fuel combustion). Given the limitations of the current data, we can only compute the $\partial/\partial z$ terms in TKE_{bp}, TKE_{sp}, and TKE_{tr}.

Since the passage of the fire-front causes a shift in the mean velocity component as well ($\overline{u}_i$), we also study the terms of the MKE budget equation in this work. The MKE budget equation is written as Stull (2012):

$$\frac{\partial (0.5\overline{u}_i^2)}{\partial t} + \overline{u}_j \frac{\partial (0.5\overline{u}_i^2)}{\partial x_j} = -g\overline{w} + \overline{u'_i u'_j} \frac{\partial \overline{u}_i}{\partial x_j} - \frac{\partial (\overline{u'_i u'_j} \overline{u}_i)}{\partial x_j} - \frac{\overline{u}_j}{\rho} \frac{\partial \overline{p}}{\partial x_j} + \nu \overline{u}_i \frac{\partial^2 \overline{u}_i}{\partial x_j^2}, \quad (2)$$

where the first term on the right-hand side represents the increase in MKE due to gravitational acceleration of vertical motions, the second term represents the interaction between TKE and MKE through shear ($-TKE_{sp}$) and accounts for the loss of MKE to TKE and vice versa, and the third term represents transport of turbulent fluxes by the mean velocity. It must be noted that the transport term in Eq. (2) represents the transport of turbulent fluxes by the mean velocity rather than the transport of MKE by turbulent fluctuations. The fourth and fifth terms on the right-hand side (not computed in this analysis) represent the production of MKE due to the acceleration of the mean flow by pressure gradients and the molecular dissipation of mean motions (Stull, 2012), respectively. Again, due to the absence of streamwise and cross-stream data resolution, we shall only compute the vertical partial derivatives ($\partial/\partial z$) in each of these terms (where applicable).

We take this opportunity to comment on the choice of 1 hour moving averages in the analysis of the sub-canopy surface fires. Moving averages are computed in this work, instead of block averages, in order to preserve the resolution of the data and the smoothness of the signal. The selection of a 1 hour time period for computing the moving averages can be explained as follows. It has been documented in the literature (Lee et al., 2004) that relatively long time periods (up to an hour) are reasonable in computing eddy fluxes. To quote from Chapter 2 of the Handbook of Micrometeorology (Lee et al., 2004): "Eddy fluxes need to be formed over a sufficiently long time that any motions that contribute to the transport can be sampled adequately. In practice, this has meant that eddy fluxes have been calculated over time periods up to an hour in duration, sufficient for several of the largest planetary–boundary–layer (PBL) scale to be sampled by the measuring system." While this argument was made in the context of turbulence in the absence of a fire, it provides a reasonable estimate for the choice of the time period of averaging in the present study. Furthermore, for the backing fires of 2011 and 2012 discussed in this study, it was found that while the time required for the firelines to pass the tower locations was of the order of minutes, the influence of the turbulence induced by the firelines at the towers lasted for approximately an hour (Heilman et al., 2015). One-hour moving averages generate a sufficiently smooth slowly-varying component for the velocity and temperature signals, which can be treated as the larger-scale atmospheric flow upon which the fire-induced fluctuations (u'_i, T') "ride". However, it is later seen from the MKE budget terms that the fire noticeably affects the mean flow even if we use a time window as conservative as 1 hour to separate the effects of the fire from the ambient flow. This, incidentally, gives

us the advantage of being able to track the "new" mean state during FFP.

Note that, in contrast to the present study, previous studies have computed block averages on the scale of a minute. Furthermore, they computed perturbations during the FFP period based on pre-FFP block means. That approach, in effect, treated all the coherent high- and low-frequency velocity and temperature variations during the FFP period as fire-induced turbulence, thereby presuming no change in the ambient atmospheric conditions during the FFP period. Moreover, the overbar terms can be very sensitive to the averaging scheme and time window. We have, therefore, included some information on the possible differences arising from using different averaging time windows in the form of a sensitivity analysis in the attached Supplementary Information.

The analysis of the grassland fire requires a slightly different approach. Only 1 hour of experimental data are available for the grassland fire. This makes it difficult to compute the slowly-varying parts (1 hour moving means) of the velocity components and temperature as done for the sub-canopy surface fires, which is in turn used to compute the turbulent fluctuations. Another approach to compute the fluctuations would be to remove the 1 hour block mean obtained from the entire time series. However, as seen in Table 1, the spread-rate and intensity of the grassland fire is one to two orders of magnitude higher than the spread-rates and intensities of the sub-canopy surface fires. Moreover, the fire-induced turbulence intensity was found to be four to five times greater than the ambient atmospheric turbulence (Clements et al., 2008). Removing the 1 hour block mean to obtain the fire-induced turbulent fluctuations would have resulted in their underestimation during FFP. The relatively high intensity and spread-rate of the grassland fire suggests that the time scale of the influence of the fire at the measuring tower is comparatively much shorter (presumably by one to two orders of magnitude), so that fire-induced changes can be considered entirely as turbulence without attributing any change to the mean state of the atmosphere. Therefore, in the analysis of the grassland fire, mean quantities are obtained by taking a block average of the first 40 minutes (pre-ignition time duration) of velocity and temperature data, as opposed to taking a 1 hour block average. Turbulent fluctuations are obtained by subtracting these pre-fire means (denoted by U, V, W, and T_m for the streamwise velocity, cross-stream velocity, vertical velocity, and temperature, respectively) from the time series for each corresponding physical quantity discussed here: $u' = u - U$, $v' = v - V$, $w' = w - W$, and $T' = T - T_m$. Note that the absence of 1 hour moving means of the velocity and temperature data in this case hinders us from computing the MKE budget terms for the grassland fire, which could have been useful for comparison with the sub-canopy surface fires. Next, we recast Eq. (1) (the TKE budget equation) for the grassland fire as follows:

$$\frac{\partial \overline{e}}{\partial t} + U_j \frac{\partial \overline{e}}{\partial x_j} = \delta_{i3} \frac{g}{T_m} \overline{u_i' T'} - \overline{u_i' u_j'} \frac{\partial U_i}{\partial x_j} - \frac{\partial \overline{u_j' e}}{\partial x_j} - \frac{1}{\rho} \frac{\partial \overline{u_j' p'}}{\partial x_j} - \varepsilon, \qquad (3)$$

Here, 1 hour moving means of the velocity components and temperature, i.e. $\overline{u}_i$ ($\overline{u}$, $\overline{v}$, $\overline{w}$) and $\overline{T}$, of Eq. (1) have been replaced by the pre-fire means, i.e. U_i (U, V, W) and T_m, in Eq. (3). Furthermore, the overbar in Eq. (3) represents 1 minute moving means. Moving means are computed as opposed to block averages to smoothen the time series associated with each term in order to facilitate drawing inferences on coherent structures. Moreover, for the high-spread-rate, high-intensity grassland fire (one to two orders of magnitude higher than those for the sub-canopy surface fires as seen from Table 1) a sufficiently short time scale must be defined for the averaging process to isolate the influence of the fire at the measuring tower. Since the time duration pre-, during, and post-FFP is 2 minutes each, a time scale longer than say, 4 minutes, would obfuscate the details of the turbulence pre-, during, and post-FFP upon averaging. The averaging time scale is chosen to be 1 minute in order to be consistent with an earlier publication by Clements et al. (2008).

3. Data overview

As mentioned above, tower-based data from four experimental fires are used in this study. We refer to the 2011 and 2012 backing surface fires beneath the canopy in the New Jersey Pinelands National Reserve (NJPNR) as NJ2011 and NJ2012, the 2019 heading surface fire beneath the canopy in the NJPNR as NJ2019, and the heading surface fire from the FireFlux experiment in the grasslands of Texas (Houston Coastal Center) as TX2006. The 2019 burn unit is located at the Silas Little Experimental Forest within NJPNR, New Lisbon, New Jersey. For the sub-canopy burns, averaged half-hourly ambient wind velocity data in the streamwise and cross-stream directions are taken from nearby AmeriFlux towers: the Cedar Bridge Tower for NJ2011 and the Silas Little Experimental Forest Tower for NJ2012 and NJ2019. These data are provided by Clark (2016a,b) and Heilman et al. (2021b); they are shown in Fig. 1 for reference and comparison with the 1 hour moving means of the measured horizontal velocity components.

For NJ2011, NJ2012, and TX2006, experimental burn data obtained from a single meteorological tower are studied in each case. For NJ2019, data obtained from two meteorological towers, i.e. the West Tower and a Control Tower, are studied for the entirety of this paper. The Control Tower is located outside the burn unit, 185 m away from its northern edge (Heilman et al., 2021b). This can also be seen in Fig. 1 of ref. Heilman et al. (2021b), which describes the burn unit and the location of the measurement towers. Measurement heights for each burn are shown in Table 1. It must be noted that the fuel consumption during the forest (sub-canopy) burns differed from each other. While NJ2011 occurred in a pine-dominated region, NJ2012 and NJ2019 occurred in an oak-dominated region. Although fuel loading of the forest floor was similar in both cases, consumption was relatively low in the oak-dominated burns. This is typical of hardwood-dominated forests: fuel consumption is usually less than that in forests with more pine trees and saplings.

For a complete description of the burn experiments, including but not limited to detailed illustrations of the burn plots, their ignition lines, and the respective directions of fireline propagation relative to the ambient winds, we refer the reader to the works of Clements et al. (2007, 2008), and Heilman et al. (2015, 2017, 2019, 2021a,b). Most of the important features of these four sets of data are summarized in Table 1. Note that although the pre-, during, and post-FFP periods indicated in Table 1 bear some similarity to the corresponding periods defined in the works mentioned above, they are not exactly the same.

4. Results

4.1. Surface fires under a tall vegetation canopy

4.1.1. Mean velocity and temperature

We first focus on the mean velocity components of the backing surface fires, NJ2011 and NJ2012 (Figs. 1(a)–(b)). In both years, $\overline{u}_{20}$ follows similar patterns as the ambient streamwise wind velocity (Figs. 1(a)(i) and 1(b)(i)). In 2011, it is seen that $\overline{u}_{10}$ and $\overline{u}_3$ are of similar magnitude during the daytime before FFP (Fig. 1(a)(ii)), since the canopy elements provide a momentum sink to the ambient wind. The average plant area density in the lower half of the canopy was much higher for the 2011 burn plot as compared to the 2012 burn plot (Heilman et al., 2017), making this effect stronger in 2011. Moreover, the mean streamwise shear ($\partial \overline{u} / \partial z$) is the highest at $h = 20$ m where $\overline{u}$ is the highest among the three heights. The high mean streamwise shear and the inflection point near the canopy top should lead to the formation of canopy-scale eddies at $h = 20$ m, the most dominant of which are known to be sweep-like momentum-flux events (Raupach et al., 1996). This is also true for NJ2012. The intermittent increase in $\overline{u}_{20}$ is attributed to intermittent gusts for both years; however, the magnitude of $\overline{u}_{20}$ throughout the day is higher in 2012 than in 2011, which is conducive to the higher spread-rate observed for NJ2011.

Table 1

Summary features for the prescribed sub-canopy backing fire experiments (NJ2011, NJ2012), prescribed sub-canopy heading fire experiment (NJ2019), and the prescribed heading grassland fire or FireFlux experiment (TX2006) analyzed in this study Clements et al. (2007, 2008), Heilman et al. (2019, 2021a).

Feature	NJ2011	NJ2012	NJ2019	TX2006 (FireFlux)
Date	20 March 2011	6 March 2012	13 March 2019	23 February 2006
Location	New Jersey Pinelands	New Jersey Pinelands	New Jersey Pinelands	Houston Coastal Center
Plot Size	107 ha	97 ha	11 ha	40 ha
Overstory Vegetation	Pitch Pine, Mixed Oak	Pitch/Shortleaf Pine, Mixed Oak	Mixed Oak, Pitch/ Shortleaf Pine	–
Measurement Heights (AGL)	3 m, 10 m, 20 m	3 m, 10 m, 20 m	3 m, 10 m, 20 m	2 m, 10 m, 28 m, 42 m
Overstory Vegetation Height	18–23 m	18–23 m	$\approx$ 19 m	–
Understory/ Grass Vegetation	Blueberry, Huckleberry, Scrub Oak	Blueberry, Huckleberry, Scrub Oak	Blueberry, Huckleberry, Bear, Blackjack, Oak sedges, Mosses	Tall-grass prairies: Big and Little Bluestem, Long Spike Tridens
Understory/ Grass Vegetation Height	1.0 m	0.7 m	1.5 m	1.5 m
Surface Fuel Loading	1.485 kg/m^2	1.104 kg/m^2	1.347 kg/m^2	1.08 kg/m^2
Ambient Wind Direction	NE-SE (45–135°)	SW-NW (225–315°)	SW (228 °)	NE (45°)
Fire Intensity	325 kW/m	52 kW/m	179 kW/m	3200 kW/m
spread-rate	1.50 m/min	0.33 m/min	1.7 m/min	40.8 m/min
Flame Length	1.0 m	0.5 m	< 2 m	5.1 m (2 m near tower base)
Fuel Consumption	696 g/m^2	507 g/m^2	337.7 g/m^2	972 g/m^2
Time of ignition	08:55 EST (09:55 EDT)	09:30 EST	14:45 LT	12:43 LT
Stipulated pre-FFP time	13:35–14:05 EST (14:35–15:05 EDT)	14:52–15:22 EST	14:50–15:20 LT	12:44:00–12:46:00 LT
Fire-front-passage (FFP) time	14:05–14:35 EST (15:05–15:35 EDT)	15:22–15:52 EST	15:20–15:50 LT	12:46:00–12:48:00 LT
Stipulated post-FFP time	14:35–15:05 EST (15:35–16:05 EDT)	15:52–16:22 EST	15:50–16:20 LT	12:48:00–12:50:00 LT

Next, note the pronounced increase in the mean cross-stream wind speed at all heights during and after FFP (1405 EST onwards) in 2011. This increase is most pronounced at $h = 20$ m (in $\overline{v}_{20}$), where cross-stream wind speeds exceed 2.5 m/s. According to Heilman et al. (2015), ambient winds (with magnitudes less than 2.5 m/s during the experiment) varied between northeasterly and southeasterly (while the cross-stream direction is N-S), suggesting higher energy in the streamwise (westward) direction. Moreover, the ambient cross-stream wind velocity (Fig. 1(a)(i)) shows a decreasing trend pre-, during and post-FFP at the measurement tower. This suggests that the increase in $\overline{v}_{20}$ is affiliated with the fire, as opposed to ambient wind conditions. Additionally, it is worth mentioning that there was some pine crown torching scattered throughout the stand during the NJ2011 burn, which was evident from a post-burn visual inspection. In particular, there was an area dominated by pitch pine within 15–20 m of the measurement tower that crowned in addition to surface combustion. This would have induced strong horizontal velocity gradients, contributing to the observed increase in $\overline{v}_{20}$ during and after FFP in 2011.

In 2012, $\overline{u}_{20}$ demonstrates the presence of intermittent gusts (as mentioned above) from the late morning through early evening. Intermittent gusts are also observed in $\overline{v}_{20}$ during the early and late evening (after 1400 LT). We shall allude to this again in Section 4.1.3. Unlike in NJ2011, the mean cross-stream wind velocity ($\overline{v}$) does not exhibit a very obvious response to the fire-presence (1522 EST onwards). Rather, $\overline{v}_{20}$ follows the ambient cross-stream wind velocity pattern as seen in Fig. 1(b)(i). This is due to the lower intensity of NJ2012 compared to the NJ2011 and lack of crown torching in the former. Other observations regarding the mean streamwise and cross-stream wind for both backing fires have already been documented in previous works (Heilman et al., 2015, 2017, 2019).

In both years, the mean vertical velocity ($\overline{w}$) during the daytime before FFP is an order of magnitude lower than the magnitudes of $\overline{u}$ and $\overline{v}$ (Figs. 1(a)(iv) and 1(b)(iv)); this is expected because of no subsidence (or no penetration at the surface). However, for the more intense NJ2011, $\overline{w}_{20}$ shows a marked increase during FFP, followed by a marked decrease to the negative side after FFP. The mean vertical wind is also seen to sink at $h = 3$ m and 10 m after FFP. This is indicative of the strong effects of fire-induced buoyancy causing an outflux of hot air into the atmosphere aloft, followed by a compensatory

influx of air from above the canopy that gathers sufficiently high momentum under gravitational acceleration for the mean vertical wind to sweep through the upper canopy (from $h = 10$ m to 20 m) before slowing down near the surface ($h = 3$ m). An influx of ambient air is also seen near the canopy top ($\overline{w} < 0$) during and post-FFP in 2012 without being preceded by a strong outflux, due to the lower intensity of NJ2012.

We now present our observations on the sub-canopy heading fire, i.e. NJ2019 (Figs. 1(c)–(d)). Peaks are observed in $\overline{u}$ at the West Tower (Fig. 1(c)(ii)), at all heights during FFP (between 1520 and 1550 LT). A similar peak is observed for $\overline{u}_{20}$ at the Control Tower (Fig. 1(d)(ii)) around that time. However, the peak in $\overline{u}_{20}$ is higher at the West tower, indicating that some increase is attributed to FFP. This is followed by a decreasing trend in $\overline{u}_{20}$ during FFP as the mean streamwise wind interacts with the ambient westward-moving sea breeze from the Atlantic coast (as noted by Heilman et al., 2021b), which has a component in the negative streamwise direction. This decrease in $\overline{u}_{20}$ is also observed at the Control tower during that time (after 1520). After 1600 LT, the ambient winds undergo a southerly shift (Figs. 1(c)(i) and 1(d)(i)). Following this shift, $\overline{u}_{20}$ becomes very low in magnitude at both the West and Control Towers, and increased magnitudes of the mean cross-stream wind velocity ($\overline{v}$) are seen at all heights, at both towers, after 1600 LT, i.e. sometime after FFP at the West Tower.

Again, the mean vertical velocity at both, the Control and West towers is an order of magnitude lower than the horizontal components (Figs. 1(c)(iv) and 1(d)(iv)); however, an increase in magnitude is seen for $\overline{w}_3$ at the West tower both during FFP (downward between 1520 and 1550 LT) and after FFP (upward after 1600 LT). Since the magnitudes of $\overline{w}_{10}$ and $\overline{w}_{20}$ are relatively low during those times, we expect this to represent a redistribution of mean kinetic energy within the canopy itself. The air seems to accelerate under gravity as it sinks to $h = 3$ m during FFP (1520 to 1550 LT). This is followed by strong updrafts, as seen from the larger magnitude of $\overline{w}_3$, due to buoyancy from residual fuel combustion after FFP (after 1600 LT and onward). Contrarily, the mean vertical wind accelerates downward under gravity at the Control Tower after 1600 LT, following an influx of ambient wind from the atmosphere aloft. We will revisit the mean vertical velocity when we discuss the MKE budget terms in Section 4.1.3.
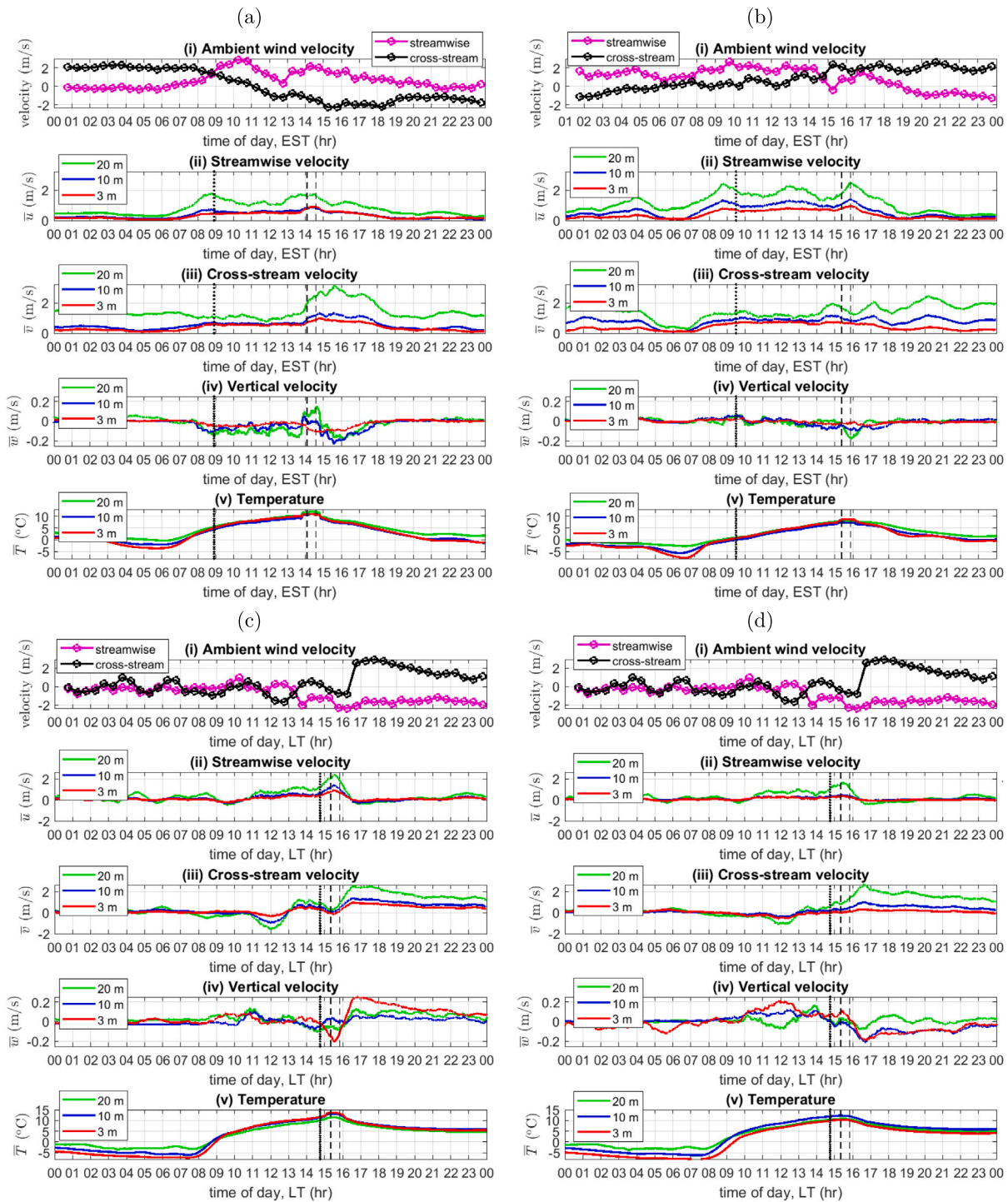
Fig. 1. (i) Ambient wind velocity recorded by nearby AmeriFlux towers. One-hour moving means of the measured (ii) streamwise velocity ($\overline{u}$), (iii) cross-stream velocity ($\overline{v}$), (iv) vertical velocity ($\overline{w}$), and (v) temperature ($\overline{T}$) for the following cases: (a) NJ2011, (b) NJ2012, (c) West Tower (NJ2019), and (d) Control Tower (NJ2019). Vertical dotted lines indicate ignition times. Vertical dashed lines delineate FFP times in (a), (b), and (c), and the West Tower FFP time in (d).

4.1.2. Wind-rose statistics

While the 1 hour moving means explored in the previous section are useful in studying the evolution of the slowly-varying mean, a first-order statistical analysis of the horizontal velocity components is required for insights into the frequency and direction of the strongest turbulent fluctuations a few minutes before, during, and after FFP. This is achieved with the help of a 2D histogram plotted on a wind compass, plotted using *WindRose* in MATLAB (Pereira, 2022). This function groups velocity data from a time series into classes based on

their magnitude, while preserving their direction relative to the positive streamwise direction. Note that zero degrees (along $\hat{\imath}$) represents the positive streamwise direction on the wind rose in each scenario.

Interesting observations can be made from the wind-rose statistics for the backing surface fires. As seen from Figs. 2(a)–(b), a shift is seen at $h = 20$ m in 2011 from high streamwise variability pre-FFP (1335 to 1405 LT) to high cross-stream variability during FFP (1405 to 1435 LT) and post FFP (1435 to 1505 LT). This corroborates well with the increase in the magnitude of $\overline{v}_{20}$ as seen in Fig. 1(a)(iii). In fact, the
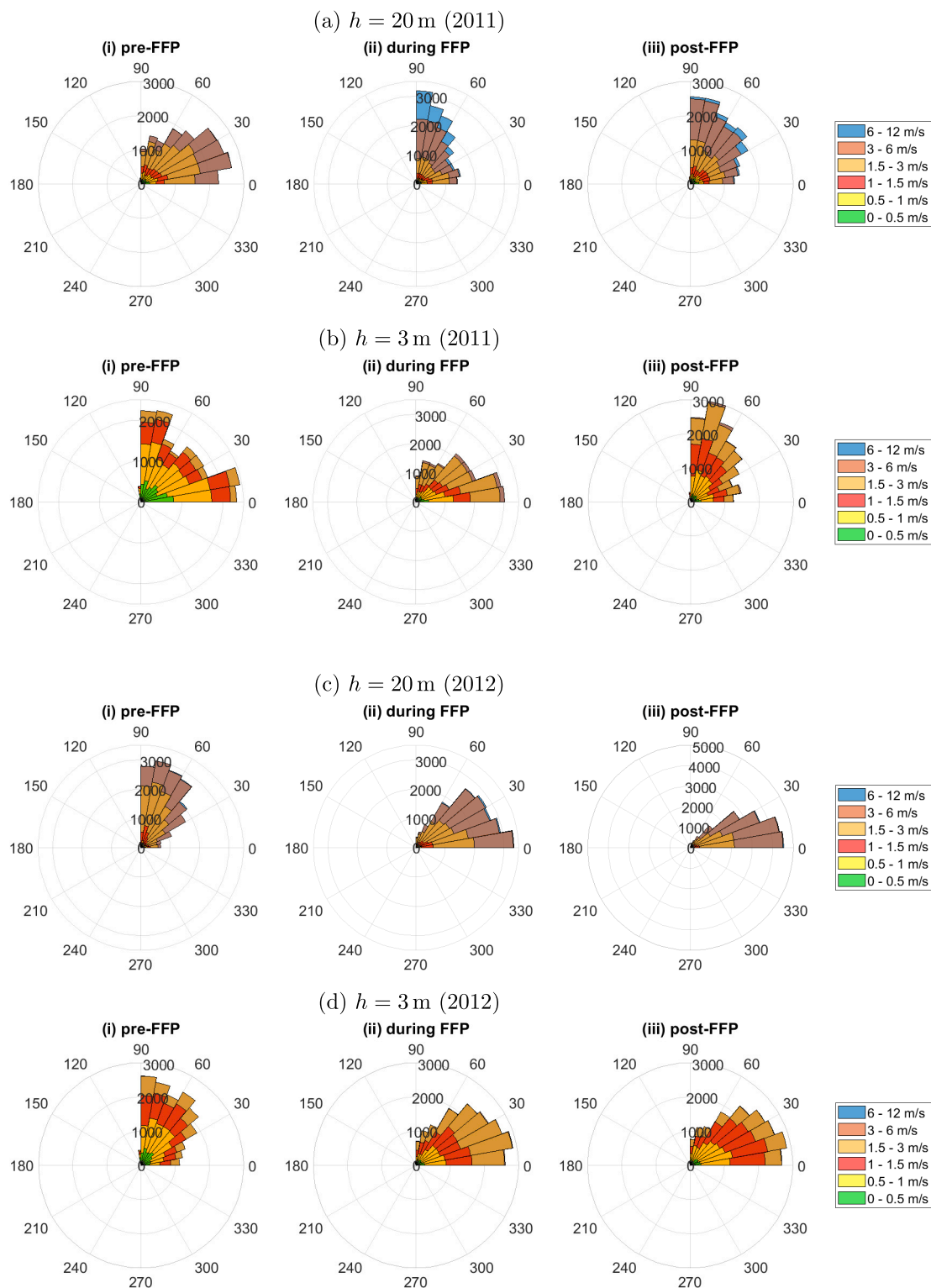
Fig. 2. Total horizontal velocity ($u\hat{\mathbf{i}} + v\hat{\mathbf{j}}$) wind-rose statistics for (i) pre-FFP, (ii) FFP, and (iii) post-FFP times at (a) $h = 20$ m and (b) $h = 3$ m for NJ2011, and for (c) $h = 20$ m and (d) $h = 3$ m for NJ2012. Colors represent classes of wind speed, while 0° represents the positive streamwise direction.

cross-stream winds show considerable variability in the range of 6 to 12 m/s during FFP as opposed to post-FFP (Fig. 2(a)(ii)–(iii)) suggesting that this effect is due to the presence of the flame. Comparison with the ambient cross-stream wind velocity (Fig. 1(a)(i)), which shows a decreasing trend during and after FFP at the measurement tower, also emphasizes that the increased cross-stream variability is attributed to

fire-induced entrainment. We can also attribute this to the diversion of momentum into the cross-stream direction as the streamwise wind (from the side of the unburnt fuel) competes with the air entrained by the fire from the burnt region. Additionally, crown torching in the stand, especially within 15–20 m of the measurement tower, would have also induced strong horizontal velocity gradients near the canopy
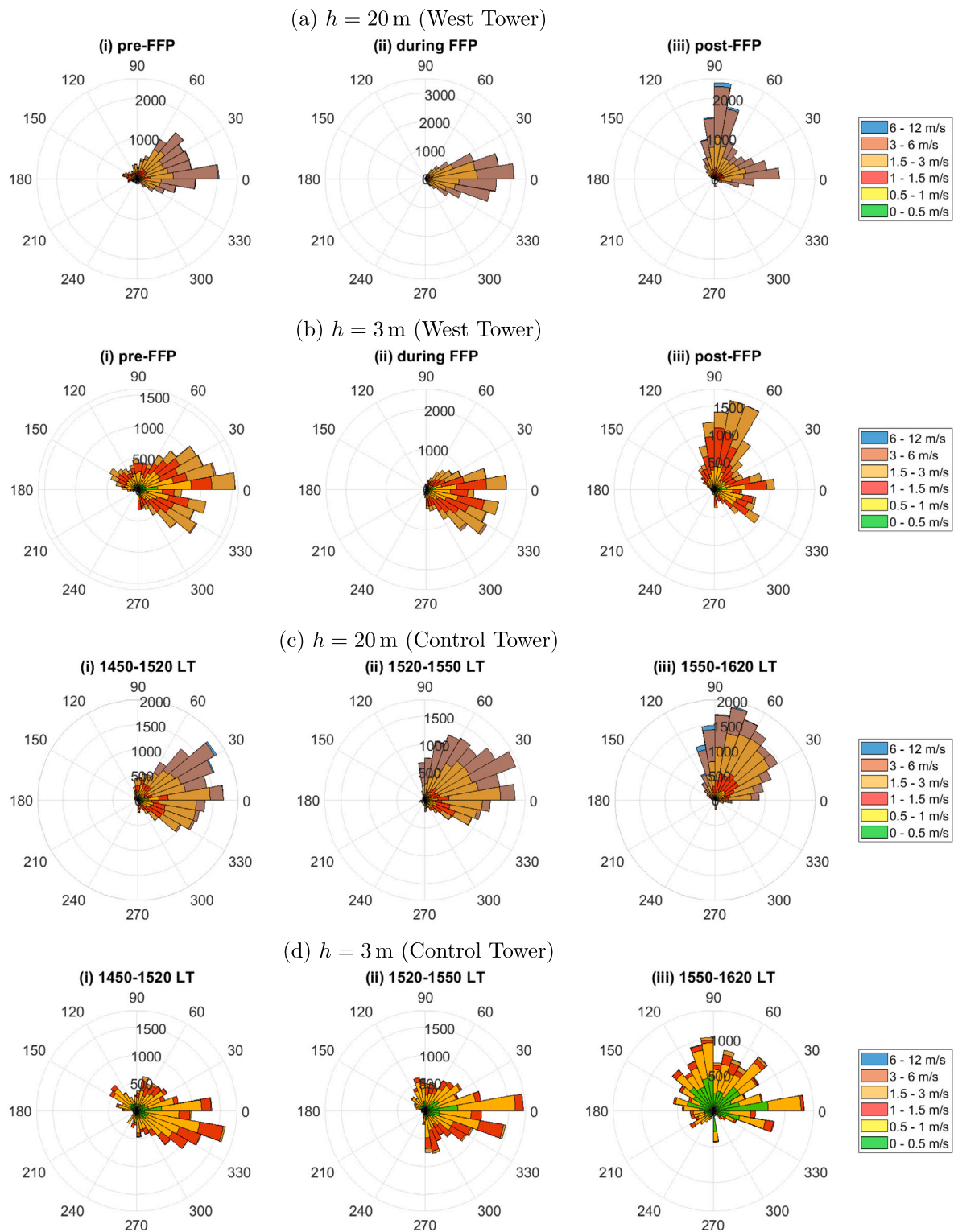
Fig. 3. Total horizontal velocity ($u\hat{i} + v\hat{j}$) wind-rose statistics for (i) pre-FFP, (ii) FFP, and (iii) post-FFP times at (a) $h = 20$ m and (b) $h = 3$ m at the West Tower for NJ2019, and at (c) $h = 20$ m and (d) $h = 3$ m, during the each of those durations, at the Control Tower for NJ2019. Colors represent classes of wind speed, while 0° represents the positive streamwise direction.

top, leading to fire-induced entrainment in the cross-stream direction near $h = 20$ m. Note that the shift in the cross-stream direction happens late at $h = 3$ m (post-FFP) since it takes a while for the cross-stream wind near the canopy top to force the wind near the ground surface.

At both $h = 3$ m and 20 m in 2012, we see a noticeable shift from high variability in the cross-stream direction pre-FFP (1452 to 1522 LT) to high variability mostly in the streamwise direction during FFP (1522 to 1552 LT) and post FFP (1552 to 1622 LT). This is attributed to the high ambient mean streamwise wind velocity as observed in

Section 4.1.1. Furthermore, the relatively lower fire intensity in 2012 does not cause noticeable entrainment in the cross-stream direction during (and post-) FFP. Contrast this with the FFP period in 2011 (Figs. 2(a)(ii) and 2(b)(ii)) during which the cross-stream winds attain speeds in the range of 6 to 12 m/s.

We now focus on the wind-rose statistics for the heading fire, i.e. NJ2019. At the West Tower, the pre-FFP, FFP, and post-FFP times are 1450 to 1520 LT, 1520 to 1550 LT, and 1550 to 1620 LT, respectively (Table 1). An increase in streamwise variability is seen at the expense of cross-stream variability at $h = 20$ m from pre-FFP to FFP times (Fig. 3(a)) possibly because of entrainment of air from the upwind side of the fire at the West Tower. The considerable variability in the cross-stream direction post-FFP is, again, attributed to the ambient wind, which undergoes a southerly shift from the FFP time to post-FFP time and has a strong cross-stream component. However, we expect the strong ambient cross-steam wind to also divert some of the streamwise eddies and momentum into the cross-stream direction. This would mean that while the cross-stream gust adds its own momentum to the canopy from aloft, it also potentially diverts some of the fire-induced turbulence near the canopy top into the cross-stream direction. Moreover, the wind statistics near the surface ($h = 3$ m in Fig. 3(b)) seems to mimic that of the higher height ($h = 20$ m) suggesting a strong forcing by the ambient post-FFP cross-stream wind.

We now compare this with the wind-rose statistics at the Control Tower (Figs. 3(c)–(d)) obtained for the pre-, during, and post-FFP times at the West Tower. In the absence of the fire, the wind rose at $h = 20$ m captures only the effects of the westward-moving sea breeze and southerly shift in the ambient wind, as evident from the increasing variability in the cross-stream wind, from pre-FFP time to post-FFP time at the West Tower (Figs. 3(c)(ii)–(iii)). It is important to distinguish the Control Tower wind-rose statistics at $h = 3$ m (Fig. 3(d)) as more disorganized from the wind-rose statistics at the West Tower for $h = 3$ m (Fig. 3(b)), especially in the post-FFP period. It seems that the presence of the flame (as it passes by and departs) at the West Tower organizes the turbulence better near the surface. For this reason, we see the wind behavior for $h = 3$ m at the West Tower mimicking that for $h = 20$ m at the West Tower post-FFP; however, at the Control Tower, the wind behavior at $h = 3$ m during this time is much more diffused compared to that at $h = 20$ m despite the strong ambient cross-stream forcing near the canopy top. Furthermore, the flame accelerates the flow near the surface as depicted by the increased streamwise wind variability in the 1.5 to 3 m/s range at $h = 3$ m, at the West Tower (Fig. 3(b)). Contrarily, the strongest wind speeds near the surface, i.e. at $h = 3$ m, at the Control Tower seldom exceed 1.5 m/s (Fig. 3(d)).

4.1.3. Turbulent and mean kinetic energy budget terms

TKE Budget Equation Terms: Fig. 4 summarizes the TKE budget terms for the sub-canopy surface fires along with the turbulent fluxes ($\overline{u'w'}$ and $\overline{v'w'}$, where u' and v' represent streamwise and cross-stream velocity perturbations, respectively). With reference to Figs. 4(a)–(b), we draw inferences for the backing fires first. We focus first on the higher-intensity fire, i.e. NJ2011 (Fig. 4(a)). At $h = 20$ m, TKE_{bp} is higher than TKE_{sp} during FFP (1405 to 1435 EST), while both attain similar magnitudes post-FFP (1435 to 1505 EST). While the effects of fire-induced buoyancy are relatively short-lived, shear production persists for a few hours after FFP. The higher-intensity fire accounts for increased buoyancy along with an increase in shear production (from pre-FFP patterns) high above the surface, i.e. near the canopy top, during FFP. Note that TKE_{sp} at $h = 20$ m largely follows the pattern displayed by $\overline{v'w'}$ (Fig. 4(a)(ii)) at that height during FFP (1405 to 1435 EST)) and after FFP (1435 EST onwards), leading us to believe that it is this component of the turbulent flux that does most of the work against the mean cross-stream wind shear ($\partial \overline{v}/\partial z$), thereby contributing the most to shear production near the canopy top. This is important in the context of the increase in mean cross-stream wind speeds at $h = 20$ m (magnitude of $\overline{v}_{20}$) after FFP as observed

in Section 4.1.1. Again, crown torching near the tower may also have some contribution in the increased magnitude of $-\overline{v'w'}$, and hence, in the increase of TKE_{sp}. Streamwise momentum eddies ($\overline{u'w'}$) also play a part in modifying the fire spread. Since it is a backing fire, fluctuations given by $u' > 0$ impede the fire spread. At $h = 20$ m, sweep-like patterns, composed of perturbations given by $w' < 0$ and $u' > 0$ (contributing to $\overline{u'w'} < 0$) lead to an import of streamwise fluctuations that impede the fire spread ($u' > 0$) into the canopy towards the lower heights. Moreover, eddies associated with $\overline{u'w'} < 0$ also act as a momentum sink for ambient wind near the canopy top. Therefore, the streamwise turbulent eddies of the canopy scale (i.e. near the canopy top) work to extract kinetic energy from the mean streamwise wind above the canopy, while also resisting the spread of the fire against the mean streamwise wind within the canopy. It must be noted here that while we may have discussed the roles of the streamwise and cross-stream momentum eddies separately, they are coupled to each other through the shear production term: the work done by one set of momentum eddies increases turbulence through shear production, which may energize another set of momentum eddies; therefore, both have an influence on each other, albeit indirectly. At $h = 10$ m (Fig. 4(a)(iv)), TKE_{bp} is the most dominant, while TKE_{sp} is minimal during FFP. This suggests that the mid-canopy region (in this case, the 10 m height) is a "conduit" for the vertical motion of energy during FFP, experiencing minimum fire-induced shear. At $h = 3$ m, both TKE_{bp} and TKE_{sp} increase during FFP, while shear production persists for a few hours after FFP (similar patterns to those observed at $h = 20$ m).

Patterns observed for the lower-intensity 2012 fire are remarkably different. At all heights, buoyancy production increases in the afternoon (pre-FFP) due to incoming solar radiation. At $h = 20$ m, there is a further but only slight increase in TKE_{bp} during FFP (1522 to 1552 EST), while TKE_{sp} does not change much from the (atmospheric) daytime pattern in the canopy. This is because the effect of the lower-intensity fire is minimally experienced near the canopy top. Instead, we observe a pattern in TKE_{sp} attributed to the intermittent ambient gusts near the canopy top, as evidenced by the fact that TKE_{sp} is patterned on $\overline{u'w'}$ at $h = 20$ m, and the well-documented knowledge that turbulence is imported via sweeps from above the canopy, which are energized by ambient gusts (Raupach et al., 1996). There is a noticeable increase in TKE_{bp} at both $h = 3$ m and 10 m during FFP (1522 to 1552 EST). However, not much fire response is seen in TKE_{sp} possibly since the understory/surface vegetation provides a momentum sink to the horizontal turbulent motion induced by the lower-intensity fire. Again, the mid-canopy region (10 m height, in this case) acts like a "conduit" for the motion of energy in the vertical direction.

We make the following observations for TKE_{tr} in 2011. With increase in w' as the fire-front approaches, which results from increased buoyancy, there is an increased loss of TKE to the above-canopy flow field via the vertical turbulent transport term. Energy loss due to this term is highest at the 20 m height, possibly due to its proximity to the above-canopy atmosphere, followed by a slightly lesser loss at the 10 m height, and finally, the least loss at the 3 m height (Fig. 4(a)). This is followed by a gain in energy at all three heights via the transport term, possibly by a reversal process after FFP. Again, the energy gained thus is highest at the 20 m height, lesser at the 10 m height, and least at the 3 m height. In contrast, in 2012, no loss to the above-canopy region is observed, since the fire intensity is lower and the increase in buoyancy (or in w') is not as pronounced as in NJ2011. There is a gain in TKE_{tr} pre-FFP, but a loss does not follow it, suggesting a vertical flux of TKE that stays within the canopy. The difference in the behavior of the vertical turbulent transport term between NJ2011 and NJ2012 is attributed to the higher intensity of the NJ2011 fire.

We now focus on the TKE budget for the heading fire, i.e. NJ2019 (Figs. 4(c)–(d)). During FFP at the West Tower, we see an increase in TKE_{sp} that is comparable with the increase in TKE_{bp} at $h = 20$ m (Fig. 4(c)(iii)). Owing to the lower intensity of the fire compared to
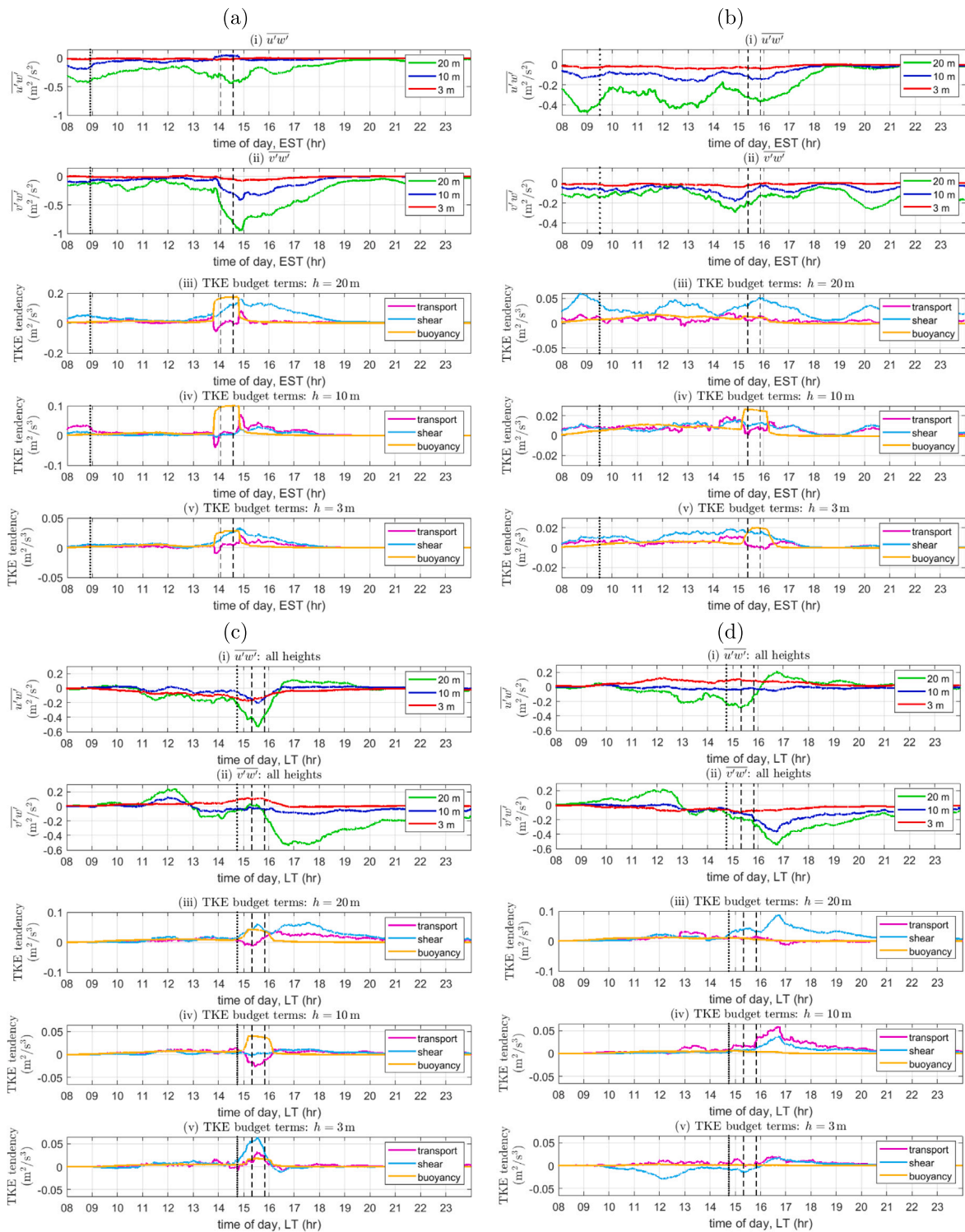
Fig. 4. (i) $\overline{u'w'}$, (ii) $\overline{v'w'}$, TKE budget terms for (iii) $h = 20$ m (iv) $h = 10$ m, and (v) $h = 3$ m for the following cases: (a) NJ2011 (b) NJ2012 (c) West Tower (NJ2019), and (d) Control Tower (NJ2019). Vertical dotted lines indicate ignition times. Vertical dashed lines delineate FFP times in (a), (b), and (c), and West Tower FFP time in (d).

NJ2011, both TKE_{sp} and TKE_{bp} at $h = 20$ m are of lesser magnitudes compared to those for NJ2011, but higher compared to those for NJ2012. The peak in TKE_{sp} is patterned on the peak in $-\overline{u'w'}$ during FFP (1520 to 1550 LT) and is, hence, attributed to the work done by the streamwise momentum flux against the mean streamwise shear ($\partial \overline{u}/\partial z$). The shear production starts to increase again, 1600 LT onwards; however, this is patterned on $-\overline{v'w'}$ (work done by the cross-stream turbulent flux against the mean cross-stream shear, $\partial \overline{v}/\partial z$) at

$h = 20$ m after 1600 LT. The increase in the magnitude of $-\overline{v'w'}$ is in turn due to the strong increase in the overall cross-stream velocity associated with the ambient wind, which must have led to an influx of turbulence into the canopy from the top. Such an increase in $-\overline{v'w'}$ (and in TKE_{sp}) is also observed at the Control Tower, reinforcing the attribution to the ambient wind as opposed to fire-induced turbulence, contrary to the case of the NJ2011 fire. Another point to note is the increase in TKE_{sp} at $h = 3$ m during FFP at the West Tower (Fig. 4(c)(v)).

It is seen that TKE_{sp} at $h = 3$ m is slightly higher compared to that at $h = 20$ m (West Tower) and is attributed to the presence of the fire. In the absence of a fire, shear production is typically insubstantial near the ground surface in a canopy environment compared to that at the canopy height. As seen from Fig. 1(c), the presence of the fire causes an increase in the mean streamwise velocity at this height ($\overline{u}_3$) resulting in an increase in the mean streamwise shear ($\partial\overline{u}/\partial z$) near the surface. Therefore, the work done by the fire-induced streamwise eddies against the mean streamwise shear ($\partial\overline{u}/\partial z$) is relatively high near the fuel-bed surface resulting in the increased shear production. This shear production associated with the fire presence acts to increase turbulence at $h = 3$ m at the West tower during FFP. Contrast this with the low-magnitude loss through TKE_{sp} at the Control Tower during this time, which suggests that shear weakly acts to decrease turbulence at $h = 3$ m.

We notice here, similar to the case of the backing fires, that TKE_{bp} is considerably higher compared to TKE_{sp} at $h = 10$ m (length scales of $h_c/2$). Again, this indicates that the mid-canopy level acts like a conduit of energy in the vertical direction during FFP. Moreover, note the loss in the turbulent transport term at $h = 10$ m at the West Tower around the time of FFP (1520 to 1550 LT). Contrast this with the weak gain in turbulent transport at the Control Tower at this height from 1520 to 1550 LT followed by a considerable gain thereafter. The loss in TKE_{tr} at the West Tower is largely because of the expulsion of TKE to the air column above $h = 10$ m, facilitated by the introduction of fire-induced turbulence from the surface (bottom of the canopy). On the other hand, the gain in TKE_{tr} at the Control Tower is because of the influx of turbulence from the top of the canopy energized by the ambient wind from the SE. For both towers, the turbulent fluxes responsible for the increased TKE_{tr} are of the scale of $h_c/2$.

The behavior of the transport term is also notable at $h = 3$ m and 20 m. During FFP at $h = 20$ m, TKE_{tr} is relatively insubstantial. However, we see a gain in the transport term ($TKE_{tr} > 0$) some time after FFP, which persists for a considerable time. This is attributed to influx of air and TKE from the atmospheric boundary layer aloft ($\overline{w'e} < 0$), following the southerly shift in the ambient wind that has a strong cross-stream component during that time. More interestingly, we see a gain in the transport term ($TKE_{tr} > 0$) at $h = 3$ m during FFP. This is because of the sinking of cooler air to this height (downward flux of turbulent kinetic energy, i.e. $\overline{w'e} < 0$) to compensate for the upward flux of warmer air due to fire-induced buoyancy ($\overline{w'T'} > 0$), resulting in a gain in TKE at this height. Overall, the turbulent transport term goes from a gain near-surface, to a loss mid-canopy, followed by inactivity near the canopy top. We expect that different heights of the air column within the canopy interact with each other through the turbulent transport term in the presence of the fire.

Mean Kinetic Energy Budget Equation Terms: The MKE shear production term ($-TKE_{sp}$), the transport term (MKE_{tr}), and the MKE buoyancy production term normalized by the numerical value of acceleration due to gravity ($MKE_{bp}/9.81$) are depicted for the sub-canopy backing and heading fires in Fig. 5. Figs. 5(a) and 5(b) depict the MKE budget equation terms for NJ2011 and NJ2012, respectively. For both years, it is observed that the transport term (MKE_{tr}) and the shear production/loss term ($-TKE_{sp}$) in the MKE equation follow a similar pattern while having opposite signs at all heights. At $h = 20$ m, both MKE_{tr} and $-TKE_{sp}$ are patterned on the magnitude of $\overline{v'w'}$ at all times in 2011, including during and after FFP (after 1405 EST) and on the magnitude of $\overline{u'w'}$ at all times in 2012, including during and after FFP (after 1522 EST). The magnitude of MKE_{tr} increases during FFP in 2011 and increases with height for both years. At $h = 3$ m, MKE_{tr} and $-TKE_{sp}$ terms cancel each other out precisely (assuming no slip at the surface). Next, we focus on $MKE_{bp}/9.81$ (which, essentially, has the numerical value of $-\overline{w}$) as shown in Fig. 5. This must be multiplied by 9.81 to obtain the actual numerical value of MKE_{bp}, which would be an order of magnitude higher; however, useful observations can be made from $MKE_{bp}/9.81$ as well. During FFP, we see a loss in this term

in 2011, due to upward flux induced by the presence of the fire, at $h = 20$ m, while there is a gain at $h = 3$ m around the same time (1405 to 1435 EST) due to sinking of air under the influence of gravity. At $h = 10$ m, this term is not very active during FFP. However, there is a gain in this term at all heights sometime after FFP (after 1500 EST), due to the influx of sinking air into the canopy. In 2012, however, there is no loss in mean kinetic energy at any height due to this term during FFP. Rather, we see a gain at $h = 10$ m and 20 m during FFP (1522 to 1552 EST) with a pronounced peak at $h = 20$ m due to increased influx of air into the canopy from the atmosphere aloft. Since NJ2012 is less intense compared to NJ2011, mean vertical updrafts are expected to be relatively weaker during FFP in 2012. Instead, there is more of a tendency for cooler ambient air to sink into the canopy via gravitational acceleration when there is an ambient gust, manifesting as a gain through MKE_{bp} at $h = 10$ m and 20 m.

Observations regarding MKE_{tr} and $-TKE_{sp}$ at the West and Control Towers for NJ2019 are very similar to those for NJ2011 and NJ2012. At the West Tower (Fig. 5(c)), MKE_{tr} and $-TKE_{sp}$ follow a similar pattern while having opposite signs. At $h = 20$ m, both terms are of lower magnitude when compared to their counterparts at this height for NJ2011, owing to the comparatively lower intensity of NJ2019. Furthermore, both MKE_{tr} and $-TKE_{sp}$ at $h = 20$ m are patterned on the magnitude of $\overline{u'w'}$ during FFP (1520 to 1550 LT) and on the magnitude of $\overline{v'w'}$ after FFP (after 1600 LT). MKE_{tr} is highest in magnitude at $h = 20$ m and lowest at $h = 10$ m, where $-TKE_{sp}$ is also of the lowest magnitude. At $h = 3$ m, MKE_{tr} and $-TKE_{sp}$ cancel each other out precisely (assuming no slip at the surface). Next, we observe that $MKE_{bp}/9.81$ has the highest variability at $h = 3$ m during and after FFP (1520 LT onward). During FFP (1520 to 1550 LT), an increase is seen corresponding to sinking of air at a relatively high vertical speed near the surface. This is followed by a persistent updraft after FFP (after 1600 LT) and hence, a persistent loss in MKE_{bp}. This loss near the surface can be attributed to residual combustion after FFP, which must induce a persistent, low-frequency updraft after FFP. A similar pattern, though with lesser variability is seen at $h = 20$ m. At $h = 10$ m, the variability in $MKE_{bp}/9.81$ (and hence in $\overline{w}$) is least, suggesting either a potential interception of, removal of energy from, or horizontal diversion of the sinking or rising mean wind at this height.

At the Control Tower (Fig. 5(d)), MKE_{tr} is patterned on the magnitude of $\overline{u'w'}$ before 1600 LT, and on the magnitude of $\overline{v'w'}$ after 1600 LT. The variability in MKE_{tr} increases with height and is lowest at $h = 3$ m, unlike at the West Tower, where it is minimal at $h = 10$ m. This shows that the transport of turbulent fluxes by the mean velocity (MKE_{tr}) decreases with proximity to the surface, as would be expected in the canopy in the absence of a fire since canopy-scale eddies give way to smaller-scale eddies near the surface. Contrary to the West Tower, we see sinking motion at $h = 3$ m and 10 m after 1600 LT. We understand this to be the result of the sinking of ambient air from above the canopy (strong ambient winds as seen in Fig. 1(d)(i)) under the influence of gravity.

Here, we provide some additional insights on the terms of the MKE budget equation. First, we comment on the net effect of MKE_{tr} and $-TKE_{sp}$. For all the canopy surface fires discussed here, MKE_{tr} is slightly higher in magnitude than $-TKE_{sp}$ and opposite in sign, so that the sum of the two terms is very close to zero. This suggests the following. While the MKE and TKE exchange kinetic energy via shear production/loss ($\mp TKE_{sp}$), the energy gained or lost by the MKE via this term is compensated by the transport of turbulent momentum fluxes by the mean velocity (MKE_{tr}). Therefore, the overall MKE tendency due to turbulent momentum fluxes becomes relatively insubstantial. Indeed, among MKE_{bp}, MKE_{sp}, and MKE_{tr}, the buoyancy production term has the most variability: it is an order of magnitude higher than the other two (because of the multiplication with 9.81). Therefore, it must be noted that the mean vertical velocity, and hence MKE_{bp}, shows a noticeable response to the presence of the fire, both during and post-FFP. Moreover, while the combined contribution of
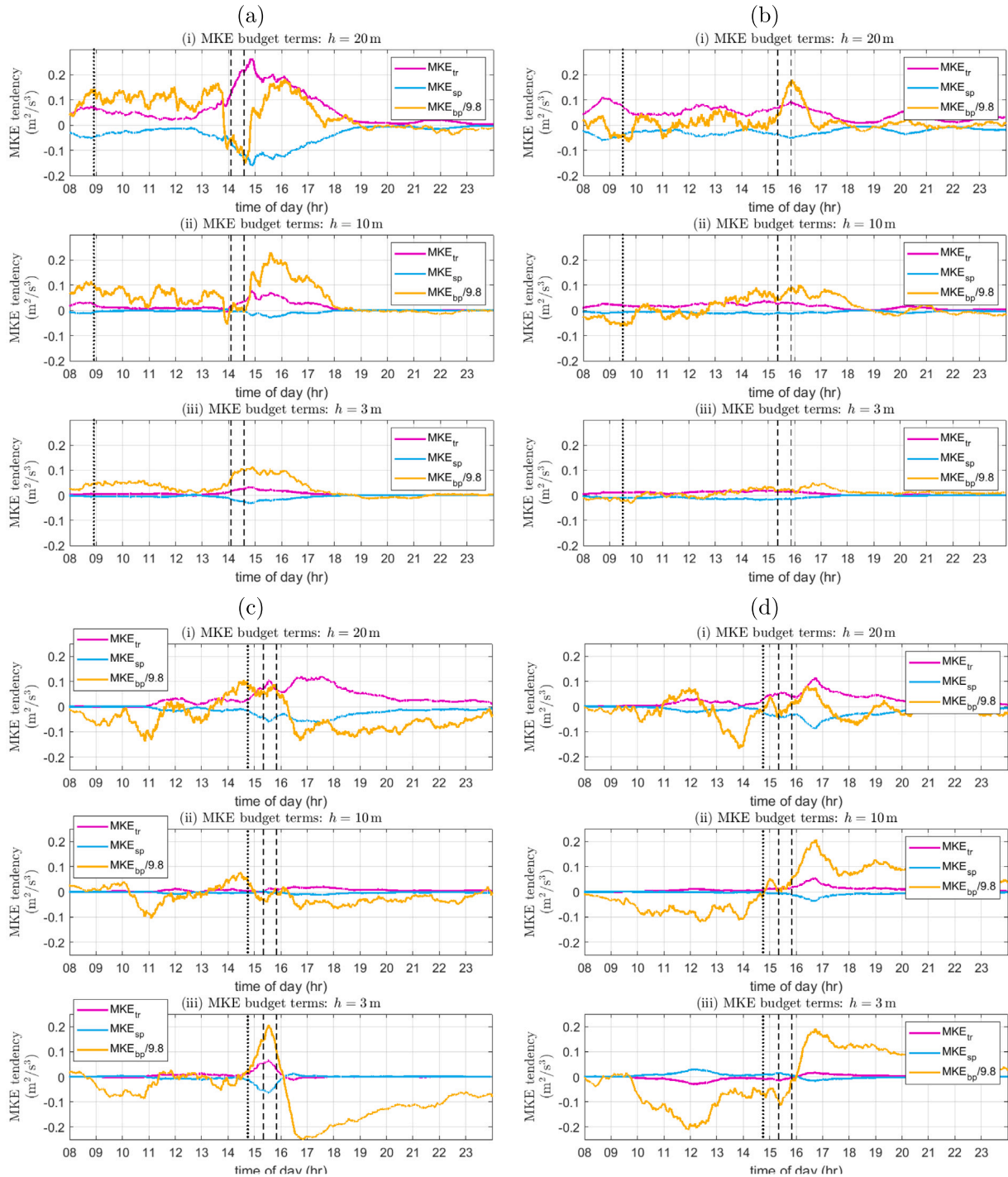
Fig. 5. MKE budget equation terms for (a) NJ2011, (b) NJ2012, (c) West Tower (NJ2019), and (d) Control Tower (NJ2019), at $h =$ (i) 20 m, (ii) 10 m, and (iii) 3 m. Vertical dotted lines indicate ignition times. Vertical dashed lines delineate FFP times in (a), (b), and (c), and West Tower FFP time in (d).

MKE_{tr} and MKE_{sp} to the overall MKE tendency is relatively low, the contribution of MKE_{bp} is considerably higher. Thus, changes in the MKE due to variation in $\overline{w}$ cannot be ignored during a fire. Again, it must be remembered that we are limited to drawing inferences from only the terms involving vertical derivatives ($\partial/\partial z$) in the MKE budget equation (Eq. (2)) due to lack of data collection in the horizontal direction. Another important observation is the consistently muted behavior of the MKE budget terms at $h = 10$ m (mid-canopy height) in all three cases, i.e. NJ2011, NJ2012, and NJ2019. This helps us envision scales for potential circulation patterns in the mean flow as the mean wind travels in and out of the canopy during the fire.

4.2. Grassland surface fire

4.2.1. Mean velocity and temperature

Fig. 6 depicts profiles of the pre-fire means (U, V, W, T_{m}) mentioned in Section 2 along with the mean kinetic energy (MKE $= 0.5(U^2 + V^2 + W^2)$) profile. The mean streamwise wind (U) increases with height (increasing profile), suggesting that $\partial U/\partial z > 0$ throughout. However, at lower heights ($h = 2$ m and 10 m), $\partial U/\partial z$ is more substantial compared to higher up ($h = 28$ m and 42 m) where $\partial U/\partial z$ is relatively much lower. Furthermore, the mean streamwise wind magnitudes are higher compared to those for the canopy fires discussed above, which
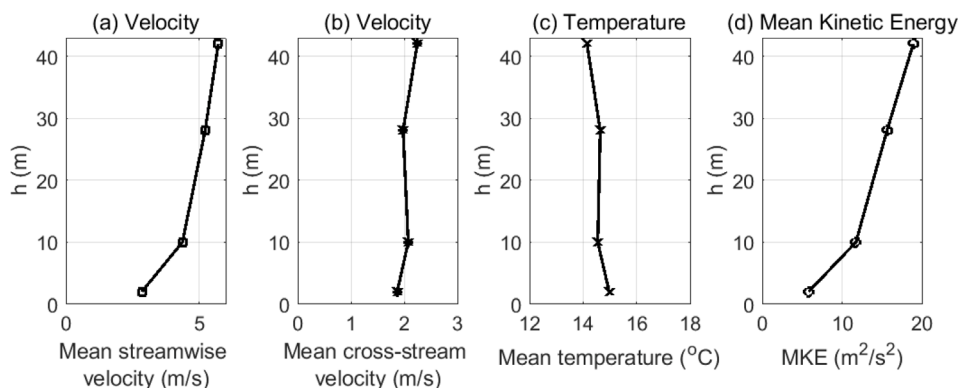
Fig. 6. Pre-ignition vertical profiles of the (a) mean streamwise velocity (U), (b) mean cross-stream velocity (V), (c) mean temperature (T_m), and (d) Mean Kinetic Energy ($(U^2 + V^2 + W^2)/2$) for TX2006.

is expected to affect the rate of spread and fire intensity accordingly. In contrast, the pre-fire cross-stream wind profile appears to be near-uniform (i.e. $\partial V/\partial z \approx 0$) for $h > 2$ m up until the fire-front reaches the measuring tower. However, $\partial V/\partial z$ is relatively high near the surface, i.e. for $h \leq 2$ m. Moreover, the near-uniform pre-fire mean temperature profile suggests a near-neutral atmosphere during the burn hour. We, therefore, expect pre-ignition convective turbulence to be relatively minimal.

4.2.2. Wind-rose statistics

Fig. 7 shows the wind-rose statistics for all four measurement heights, constructed from the pre-FFP (1244 to 1246 LT), FFP (1246 to 1248 LT), and post-FFP (1248 to 1250 LT) time intervals at the tower. We notice that the flow seems to accelerate near the surface during FFP as evidenced by the considerable variability in the 6 to 12 m/s speed range accompanied by a little variability in the 12 to 15 m/s speed range at $h = 2$ m in Fig. 7(d)(ii), which is absent in the pre-FFP time duration (Fig. 7(d)(i)). Again, this is expected to be a consequence of fire-induced entrainment from the upwind side of the flame, which accelerates the flow predominantly in the streamwise direction. This is emphasized by the fact that the variability in the 6 to 12 m/s speed range decreases noticeably post-FFP at $h = 2$ m (Fig. 7(d)(iii)), suggesting that these wind speeds attained during FFP are unlikely to be associated with ambient conditions. Similar observations can be made for $h = 10$ m (Fig. 7(c)), due to its proximity with the fire plume. In other words, the fire flame and the hot air column above it acts like a pump that accelerates the flow. Another point to note is that although the wind was known to have a detectable cross-stream component during the burn experiment (Clements et al., 2007) (also corroborated by the pre-FFP wind-rose statistics at $h = 2$ m and 10 m), the wind is dominantly aligned in the positive streamwise direction pre-FFP, during FFP, and post-FFP at the higher heights, i.e. $h = 28$ m and 42 m (Figs. 7(a)–(b). We expect this to be a consequence of entrainment by the flame from the upwind side of the fire in the streamwise direction. This entrainment is experienced pre-FFP at the higher heights since the tilting of the fire plume in the direction of the wind induces strong temperature fluctuations (a high pressure differential) at the higher heights before the arrival of the fire-front at the base of the tower.

4.2.3. Turbulent and mean kinetic energy budget terms

Turbulent Kinetic Energy Budget Terms: Before drawing on the TKE budget terms for inferences, we assess the 1 minute moving mean of the TKE ($\bar{e}$) and of the fraction of the vertical TKE ($r = 0.5\overline{w'^2}/e$) from Fig. 8(a)(i)–(ii). Note that the increase in $\bar{e}$ at $h = 28$ m and 42 m is seen earlier than at $h = 2$ m and 10 m as the fire-front approaches the tower due to tilting of the flame in the direction of the wind as observed by Clements et al. (2007, 2008). At $h = 2$ m and 10 m, $\bar{e}$ during FFP is higher than that for $h = 28$ m and 42 m, due to proximity with the fire

plume, the source of the increased turbulence. In fact, $\bar{e}$ is the highest at $h = 2$ m. Since fuels were removed around the base of the tower, $h = 2$ m represents the local flame height near the tower. The high value of $\bar{e}$, in conjunction with the low value of r at $h = 2$ m ($r \approx 0.1$) in Fig. 8(a)(ii), is noteworthy. This suggests that the horizontal fraction of TKE at $h = 2$ m is considerably higher during FFP. While this could be because of the attenuation of w' due to the proximity with the ground surface, it could also be representative of the horizontal acceleration of the flow past the flame (Fig. 7(d)) or increased entrainment from the upwind side. This horizontally accelerated flow causes the forward advection of hot gases onto unburnt fuel, which is responsible for the fire spread (also observed on laboratory scales by Finney et al., 2015). At $h = 10$ m, 28 m, and 42 m, the values of r are higher than 0.3 pre-FFP, followed by values of r less than 0.2 during FFP. This is explained as follows. The tilting of the flame in the direction of the wind increases the variability in the vertical direction at the higher heights pre-FFP by virtue of buoyancy effects. During FFP, the effect of buoyancy at the higher heights, at the tower location, is greatly reduced and much of the variability is found to be in the horizontal velocity.

Let us now examine the streamwise turbulent flux ($\overline{u'w'}$) closely (Fig. 8(b)(i)). An increase in the magnitude of the turbulent flux pre- and during FFP, caused by the presence of the fire, is seen in Fig. 8(b)(i). Typically, negative $\overline{u'w'}$ ($\overline{u'w'} < 0$) in the atmospheric boundary layer (ABL) represents a momentum sink. Two possible cases that contribute to negative $\overline{u'w'}$ (Fig. 8(b)(i)) are considered: sweep-like patterns, i.e. $w' < 0$ and $u' > 0$ and ejection-like patterns, i.e. $w' > 0$ and $u' < 0$. At all heights AGL, eddies associated with sweep-like patterns send streamwise fluctuations assisting in fire spread ($u' > 0$) to the lower heights, i.e. towards the flame at the surface ($w' < 0$). Therefore, the streamwise turbulent flux associated with sweep-like events at these heights assists in the fire spread, while also providing a momentum sink to the ambient mean wind. The effect of eddies associated with ejection-like patterns is explained as follows: in-drafts of air from the downwind side ($u' < 0$) are diverted away from the fire flame near the surface ($w' > 0$) so that they play more of a role in vertical transport rather than impeding the fire spread.

Next, we explore the influence of the streamwise turbulent flux on the TKE budget terms as shown in Fig. 8(c). First, we note that the shear production term (TKE_{sp}) at $h = 2$ m and 10 m is patterned on $-\overline{u'w'}$ at those heights. During FFP, the increase in TKE_{sp} is highest at $h = 2$ m, followed by $h = 10$ m. At both heights, this increase is higher than that at the higher heights AGL ($h = 28$ m and 42 m). This is because shear production is a consequence of work done by the turbulent fluxes (in this case, mostly $\overline{u'w'}$) against the mean wind shear (in this case, $\partial U/\partial z$). In a grassland environment, the mean streamwise wind shear is higher closer to the ground surface, as opposed to near the top of the canopy in a forested environment as discussed in Section 4.1. This accounts for the high increase in TKE_{sp} at $h = 2$ m. From $h =$
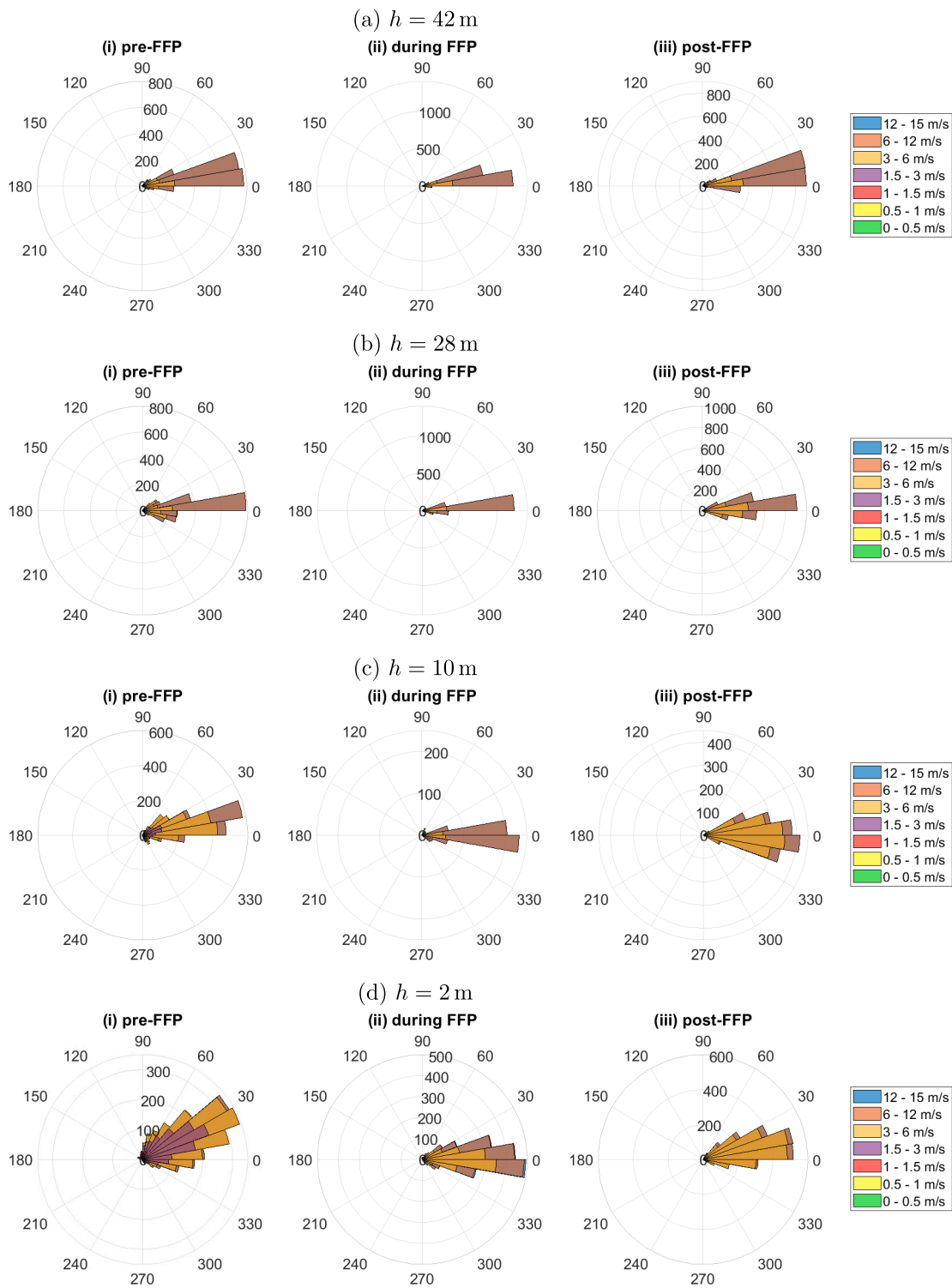
(a) $h = 42$ m

(b) $h = 28$ m

(c) $h = 10$ m

(d) $h = 2$ m

Fig. 7. Total horizontal velocity ($u\hat{\mathbf{i}} + v\hat{\mathbf{j}}$) wind-rose statistics for (i) pre-FFP, (ii) FFP, and (iii) post-FFP times at h = (a) 42 m, (b) 28 m, (c) 10 m, and (d) 2 m for TX2006. Colors represent classes of wind speed, while 0° represents the positive streamwise direction.

2 m to 10 m, the shear production decreases with height despite the increase in $-\overline{u'w'}$ since $\partial U / \partial z$ decreases with height. Higher up, both $-\overline{u'w'}$ and $\partial U / \partial z$ decrease with height; therefore, the work done by the streamwise turbulent flux against the mean streamwise wind shear is low. This suggests that shear production is associated with work done against the mean streamwise shear by the streamwise turbulent eddies that assist in pushing the flame towards the unburnt fuel, as

discussed in the previous paragraph. Since the shear production is positive ($TKE_{\mathrm{sp}} > 0$), the work done serves to remove energy from the MKE and provide it to the TKE. The resulting increase in TKE helps in sustaining the turbulent eddies that assist in the fire spread.

We also take this as an opportunity to comment on $\overline{v'w'}$. Similar to the NJ2011 fire, cross-stream eddies do seem to strengthen in response to the fire presence during FFP. However, such strengthening is only
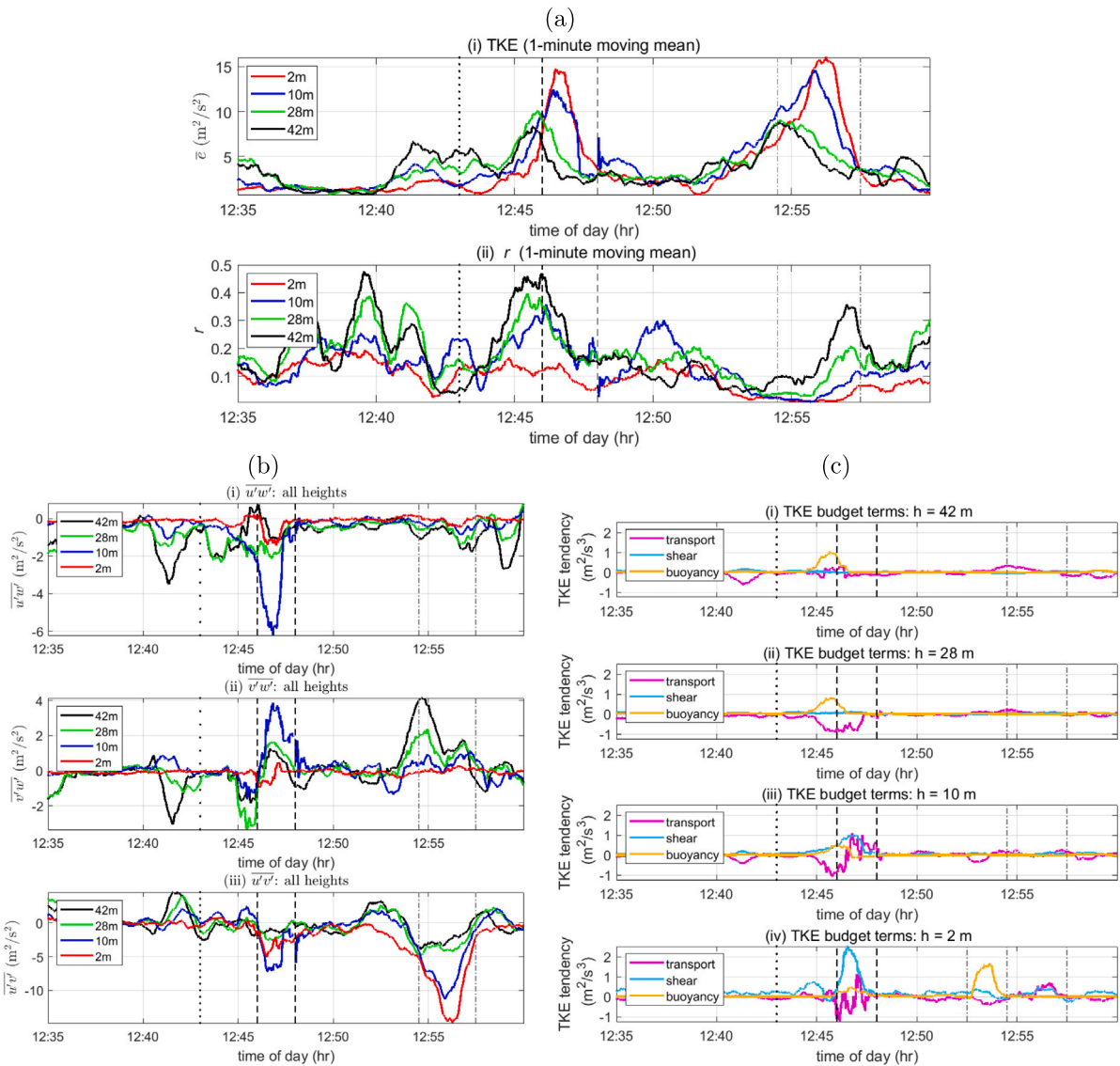
Fig. 8. For TX2006: (a)(i) One-minute moving means of the TKE and (ii) the vertical fraction of TKE (r); (b) turbulent fluxes, i.e. (i) $\overline{u'w'}$, (ii) $\overline{v'w'}$, and (iii) $\overline{u'v'}$ at all four heights; (c) TKE budget terms at h = (i) 42 m, (ii) 28 m, (iii) 10 m, and (iv) 2 m. Black dotted vertical line indicates ignition time; black dashed vertical lines delineate FFP time.

seen at $h = 10$ m. Furthermore, since the mean cross-stream wind shear is minimal ($\partial V / \partial z \approx 0$) at this height (Fig. 6(b)), the work done by the cross-stream eddies in overcoming the mean cross-stream shear is insubstantial. Consequently, the majority of shear production is associated with the work done by the streamwise eddies against the mean streamwise wind shear. Since shear production itself results in an increase in turbulence, it is possible that the cross-stream turbulent eddies at $h = 10$ m germinate from this increase in turbulence. In this manner, the cross-stream eddies appear to be coupled to the streamwise eddies at this height. Moreover, the presence of strong cross-stream turbulent eddies at $h = 10$ m is an important observation in the context of laboratory experiments documented in the literature that suggested that cross-stream eddies are vital to the advection of hot gases from the burned fuel to the unburned fuel, which effactually causes the fire to spread (Finney et al., 2015). Considering that cross-stream eddies weaken beyond this height, an estimate of the length scale associated with such eddies can also be obtained from this height. Furthermore, it is worth noting the increase in $-\overline{v'w'}$ at $h = 28$ m pre-FFP (Fig. 8(b)(ii)), which suggests a strengthening of the cross-stream eddies at the higher heights pre-FFP possibly due to the effects of flame tilting.

Additionally, we observe an increase in $-\overline{u'v'}$ during FFP (Fig. 8(b)(iii)) for the grassland fire. This indicates an increase in the

strength of horizontal turbulent eddies induced by the presence of the flame. It is known that horizontal eddies are formed as a consequence of fire-induced entrainment in the horizontal plane (Tohidi et al., 2018), which is expected to be relatively intense in an open grassland environment. We further expect these to contribute to the formation of fire-whirls or dust devils, as discussed later in this section. The increase in strength of the horizontal eddies is particularly noticeable at $h = 2$ m and 10 m and is highest at $h = 10$ m. This provides a perspective on the length scale associated with horizontal turbulent eddies during FFP, with respect to the given flame height, in a grassland environment.

Fig. 8(c) shows that shear production is more substantial as compared to buoyancy production during FFP at the lower heights AGL, i.e. at $h = 2$ m and 10 m. While the reasons for increased TKE_{sp} have been discussed above, the decreased TKE_{bp} is associated with the attenuation of the vertical velocity fluctuations (w') at these heights even during FFP due to proximity with the ground surface. However, buoyancy production is more significant compared to shear production at the higher heights AGL, i.e. $h = 28$ m and 42 m pre-FFP (Fig. 8(c)). This suggests that while the tilting of the flame in the direction of wind induces strong vertical fluctuations at the higher heights pre-FFP, thereby causing an increase in TKE_{bp}, it does not result in increased

TKE_{sp} at these heights despite the increase in the strength of the cross-stream eddies pre-FFP. Shear production at the higher heights remains insubstantial pre-FFP.

Some interesting inferences can be drawn from the very active turbulent transport term ($TKE_{tr} \neq 0$) before and during FFP. Typically, in the ABL, the turbulent transport term is not very active and equilibrium exists between viscous dissipation (ε) and shear production (TKE_{sp}). At $h = 42$ m, the turbulent transport term remains relatively insubstantial and the buoyancy production term remains the only active source of turbulence generation pre-FFP. At $h = 10$ m and 28 m we observe a loss in TKE_{tr} pre-FFP (and for some time during FFP), which is associated with an average upward flux of TKE caused due to buoyant updrafts induced by the tilted flame. This is followed by a gain at $h = 10$ m and a persistent loss at $h = 28$ m during FFP. The gain at $h = 10$ m is attributed to an incoming flux of TKE from higher heights as the effects of fire-induced buoyancy weaken at the higher heights ($h = 28$ m) along with an incoming flux of TKE from $h = 2$ m where fire-induced buoyant updrafts are still active during FFP. At $h = 2$ m, we see a similar pattern of loss in TKE_{tr} followed by a gain in TKE_{tr}.

So far, we have analyzed the turbulent fluxes and terms of the TKE budget equation for the primary burn in the domain. Let us now focus on the turbulent fluxes and TKE budget 6 to 10 minutes after FFP. Some increase in $\bar{e}$ is observed at the higher heights AGL ($h = 28$ m and 42 m) followed by a considerable increase at the lower heights ($h = 2$ m and 10 m) around this time (Fig. 8(a)(i)). The increase in $\bar{e}$ at each of these heights coincides with a drop in r to values below 0.1, indicating that it is associated with stronger horizontal turbulent fluctuations (u', v'). We also see an increase (peaks) in $-\overline{u'v'}$ between 1254:30 and 1257:30 LT at $h = 2$ m and 10 m (marked by gray dash-dotted vertical lines in Fig. 8(b)(iii)), while $\overline{u'w'}$ and $\overline{v'w'}$ remain relatively low in magnitude at these heights emphasizing the importance of the horizontal turbulent eddies over the vertical eddies in this time duration. This corroborates well with the observations by Clements et al. (2008) that associated the increase in $\bar{e}$ with the appearance of a dust devil along with horizontal turbulent eddies arising from a secondary burn of a small section of the grassland immediately upwind of the experimental plot that was ignited after the experimental (primary) burn was completed. Moreover, an increase in buoyancy production ($TKE_{bp} > 0$) is also seen at $h = 2$ m between 1252:30 and 1254:30 LT (marked by gray dash-dotted vertical lines in Fig. 8(c)(iv)) despite relatively weak w'; this is because of intense fluctuations in temperature (stronger T' than during FFP for the primary burn!) around this time at $h = 2$ m. It appears that the combined effect of residual combustion from the primary burn, including but not limited to smoldering, and flaming combustion from the secondary burn may be responsible for the increase in TKE_{bp} at the base of the 43 m tower between 1252:30 and 1254:30 LT, while the observed dust devil (and horizontal turbulent eddies caused by the secondary burn) is mainly responsible for the increase in $\bar{e}$ at this point between 1254:30 and 1257:30 LT. Additionally, signatures of buoyancy production, such as those seen at $h = 2$ m, are not seen at $h = 10$ m, 28 m, and 42 m from 1252:30 to 1254:30 LT, possibly because fluctuations in the vertical velocity (w') are weaker compared to those during flaming combustion from the primary burn. Furthermore, although horizontal wind shear leads to the increase in $\bar{e}$ from 1254:30 to 1257:30, as suggested by Clements et al. (2008), the increase in shear production (TKE_{sp}) at $h = 2$ m is relatively inappreciable (Fig. 8(c)(iv)) during that time. This is despite the increased strength of horizontal turbulent eddies as evident from the increase in the $-\overline{u'v'}$ (Fig. 8(b)(iii)). A possible explanation lies in the fact that we have not considered the contribution of the work done by the horizontal eddies towards TKE_{sp} due to lack of data collection in the horizontal plane, which impedes mean wind shear calculations in the horizontal plane ($\partial/\partial x$ and $\partial/\partial y$).

5. Discussion

Fire-atmosphere interaction comprises several simultaneous complex phenomena including but not limited to the entrainment of ambient air, the formation of strong turbulent eddies, the introduction of fire-induced turbulence (buoyancy production, shear production) from the surface and its redistribution in the air column above (turbulent transport), the injection of ambient turbulent fluxes from the canopy top, and the redistribution of mean kinetic energy in the air column. In this section, we integrate the key processes and events that have been inferred and elaborated on in the previous section. Figs. 9, 10, and 11 present brief summary pictures of the sub-canopy backing surface fire (high intensity), the sub-canopy heading surface fire, and the heading surface fire in a grassland, respectively.

Comparison with a no-fire situation suggests that the presence of an approaching flame (e.g., at the West Tower for NJ2019) tends to organize the turbulence near the surface in the streamwise direction, in contrast to the more disorganized flow in the absence of fire (e.g., at the Control Tower). The presence of the flame also leads to the entrainment of ambient air from both the upstream and downstream side of the fire. In some cases, wind entrained from the upwind side of the fire interacts with that from the downwind side and diverts momentum in the cross-stream direction as well. In the grassland fire, we see that the horizontal wind near the ground surface accelerates during FFP due to the presence of the flame, with high variability in the streamwise direction (Fig. 11). In other words, the flame acts like a pump for the wind in the streamwise direction. Acceleration of the wind past the hot air column above the flame is also seen in the case of the sub-canopy surface fires (Figs. 9 and 10). Moreover, the increase in mean streamwise wind speed past the hot air column above the flame at higher heights in the case of the sub-canopy heading surface fire (NJ2019) suggests some coupling between fire-induced buoyancy and the corresponding mean velocity components.

In all sets of sub-canopy surface fires, turbulent eddies (either streamwise or cross-stream) are found to be strongest near the canopy top (Figs. 9 and 10): strong streamwise turbulent flux is accompanied by relatively weaker cross-stream turbulent flux and vice-versa. Furthermore, it must be noted that both are coupled with each other through shear production. The highest shear production amongst the different heights in the air column is near the canopy top, attributed to the strong turbulent flux there. For the more intense sub-canopy surface fires, shear production near the canopy top is attributed to the fire and can persist for a few hours post FFP. For the relatively lower intensity sub-canopy surface fires (e.g. NJ2012), shear production is dictated by intermittent gusts and the background canopy-scale turbulence (work done by strong turbulent eddies against the mean shear). Sub-canopy surface fires seem to be affected considerably by the turbulence near the canopy top. The injection of turbulence into the canopy via sweep-like eddies ($\overline{u'w'} < 0$) near the canopy top has different connotations for backing and heading fires: the associated streamwise eddies resist the fire spread in the case of backing fires, while they assist fire spread in the case of heading fires. For the relatively more intense sub-canopy surface fires (e.g. NJ2011), cross-stream turbulent fluxes become prominent. In the grassland fire, both cross-stream and streamwise eddies strengthen with height before attaining a maximum (in this case, at the 10 m height) and starting to weaken with height (Fig. 11). The strengthening of cross-stream eddies is important in the context of recent laboratory-scale experiments that suggested that cross-stream eddies advect hot gases forward onto unburnt fuel (Finney et al., 2015). Albeit on a management-scale, the strong cross-stream eddies seen here could similarly participate in fire spread in the grassland environment and the height at which these eddies are the strongest provides the associated vertical length scale (relative to the flame height). Furthermore, we infer that the downwash from strong streamwise eddies of this scale ($\overline{u'w'} < 0$) also participates in the fire spread by pushing hot gases onto the unburnt fuel ($w' < 0$ and $u' > 0$). This is in
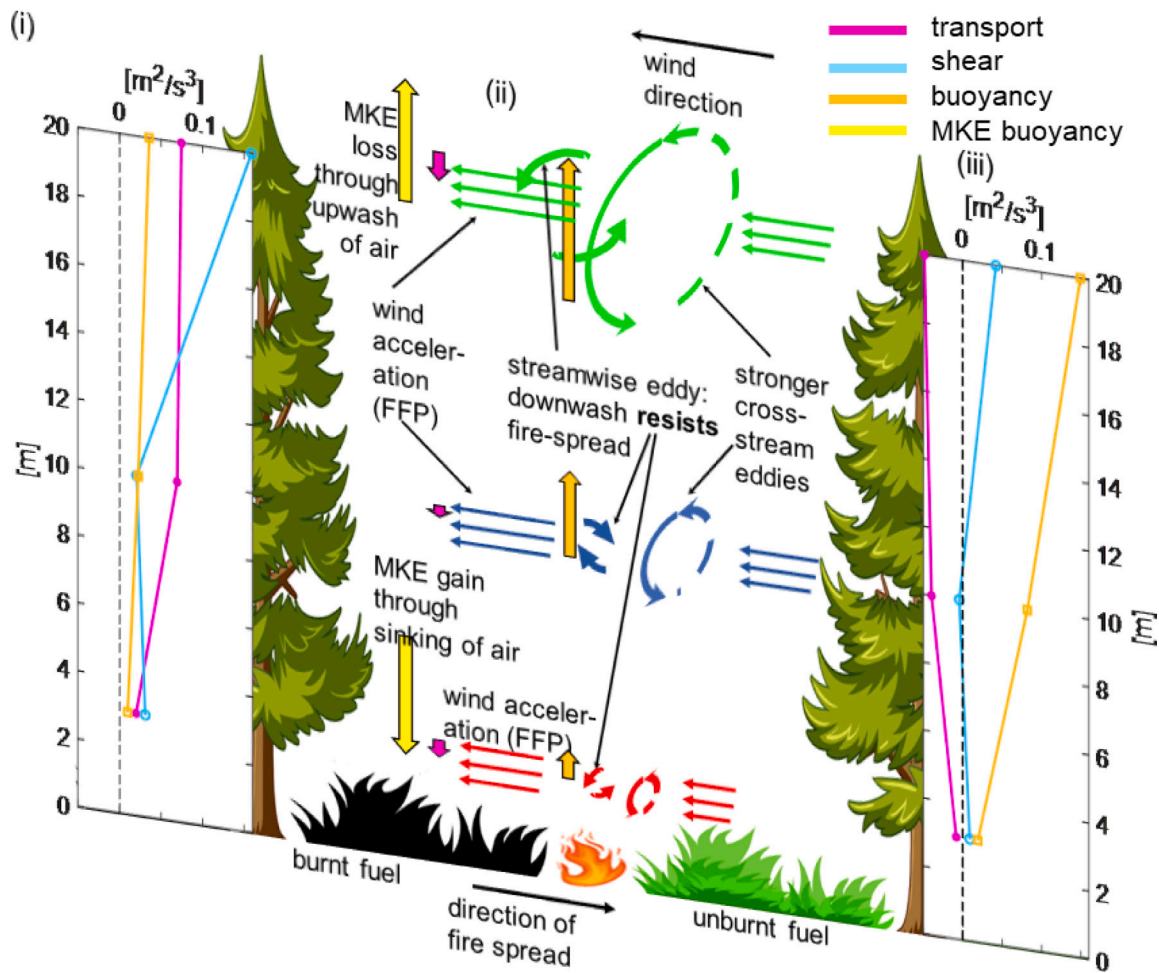
Fig. 9. A brief summary of the turbulent processes in the 2011 sub-canopy backing surface fire (NJ2011) along with profiles of the TKE budget terms for a time instant in the (i) post-FFP period and (iii) pre-FFP period. Arrows are not to scale. (Vector figures of the pine tree, black bush, and green bush, on one hand, and flame, on the other, taken from *www.vecteezy.com/free-vector/nature* and *www.vecteezy.com/free-vector/flame*, respectively).

consonance with the results of Desai et al. (2022) pertaining to a small-scale grassland fire, which suggested that vortices generated from the entrained air push hot gases outward away from the flame. The near-surface wind also seems to accelerate past the flame: also an observation that matches with those from Desai et al. (2022). It is noteworthy that the phenomena seen in the grassland fire from this paper, while pertaining to a large-scale prescribed burn, conform to those from a small-scale burn experiment on grassland fires. Contrary to the case of the sub-canopy surface fires, shear production in grassland fires is highest near the surface. This shear production is correlated to the forward advection of hot gases and the upwash of indrafts from the downwind side. Shear production then decreases with height (Fig. 11), despite the increase in the strength of the streamwise eddies; this is because the mean streamwise wind shear reduces with height so that the work done by the streamwise turbulent eddies against the mean streamwise wind shear is low.

In the absence of a fire, the shear length scale for a canopy is typically of the order of $h_c/2$ (Raupach et al., 1996). Our analysis shows that shear production increases with height in the absence of a fire (at the Control Tower in 2019). However, at length scales of half the canopy height in the presence of a surface fire, the buoyancy production far exceeds the shear production. This makes us envision the mid-canopy height as a channel for vertical transport of kinetic energy during FFP and further emphasizes the importance of length scales of $h_c/2$. In the grassland environment, vertical length scales are dictated by the height at which the turbulent eddies become the strongest during FFP ($h = 10$ m in this case) as evidenced by the increased magnitude of

the turbulent fluxes ($-\overline{u'w'}$ and $\overline{v'w'}$), seen in Fig. 11. The grassland fire data also show the presence of horizontal turbulent eddies that increase in strength (increase in magnitude of $-\overline{u'v'}$) up to $h = 10$ m. We would expect this height to vary depending on the fire intensity, flame height, and wind speed. Another measure for the shear length scale in a grassland environment during FFP can be obtained from the height at which the shear production begins to drastically reduce with height; in this case, this is achieved at a height above $h = 10$ m.

It is easy to see that buoyancy production increases with height in both environments due to the increased variability in the vertical wind velocity fluctuations (w') with height. However, the height to which the buoyancy production continues to increase is determined by the fire intensity. Another notable aspect is the role of the turbulent transport term. It is a well-documented observation that the turbulent transport term is active within the canopy as opposed to the ABL aloft where equilibrium generally exists between viscous dissipation and shear production (Raupach et al., 1996). This is also demonstrated by the active turbulent transport term (gain) at a height of $h_c/2$, at the Control Tower in 2019. Much like how sweeps inject turbulence into the canopy from the ABL aloft, fire injects turbulence into the canopy from the surface. For more intense surface fires beneath the canopy, it seems that while there is a gain in TKE through buoyancy production, there is a loss in TKE (mid-canopy and/or at other heights) due to expulsion of TKE to the ABL aloft via the turbulent transport term (pre- and post-FFP profiles in Figs. 9 and 10). Such an expulsion is compensated by a reversal process where there is an influx of TKE via the turbulent transport term. The transport term in the grassland fire
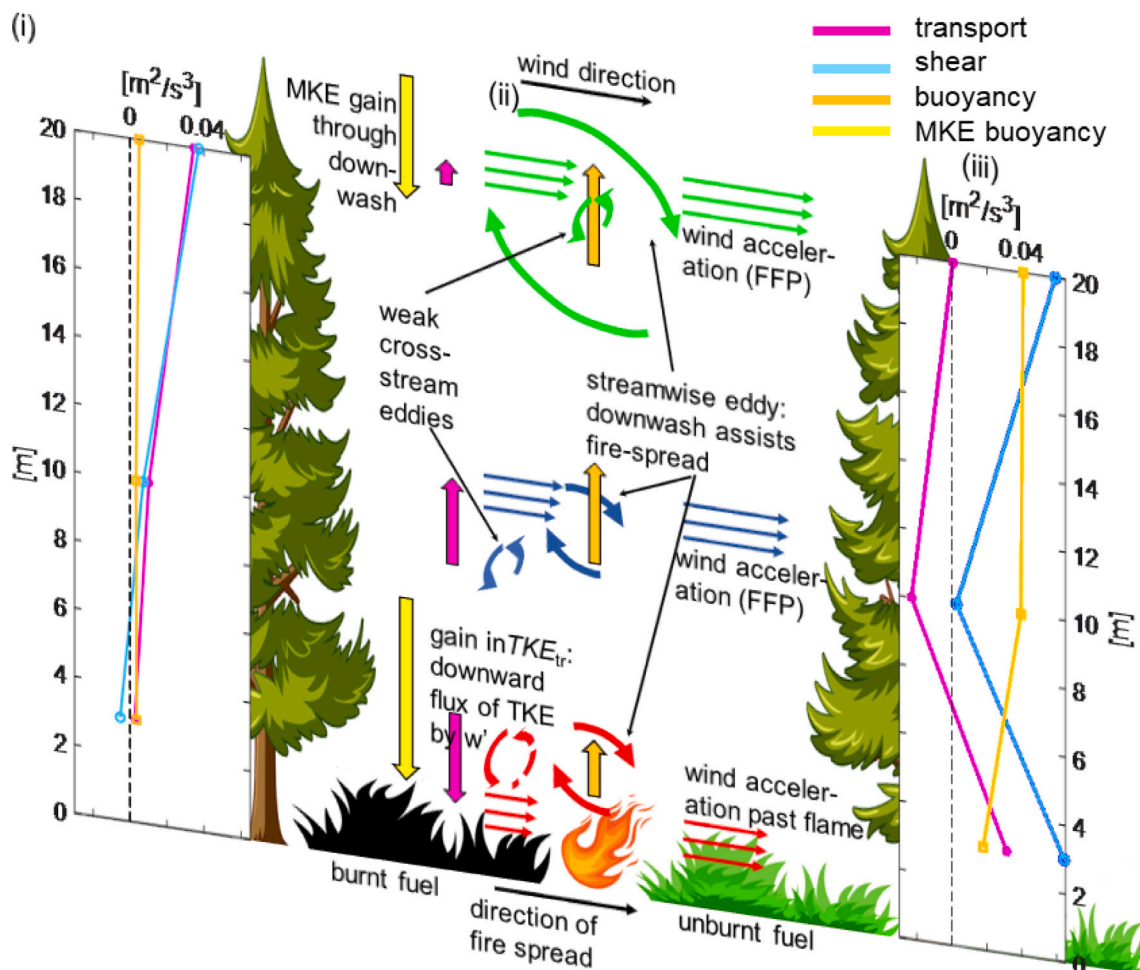
Fig. 10. A brief summary of the turbulent processes in the 2019 sub-canopy heading surface fire (NJ2019) along with profiles of the TKE budget terms for a time instant in the (i) post-FFP period and (iii) pre-FFP period. Arrows are not to scale. (Vector figures of the pine tree, black bush, and green bush, on one hand, and flame, on the other, taken from *www.vecteezy.com/free-vector/nature* and *www.vecteezy.com/free-vector/flame*, respectively).

mimics this behavior up to a certain height above the surface ($h = 10$ m in this case) relative to the flame height (Fig. 11). Thus, the turbulent transport term actively participates in the vertical redistribution of TKE in the air column and its behavior can be used to determine important vertical length scales. However, it must be noted that we have not been able to include the effects of the turbulent transport terms involving horizontal gradients ($\partial/\partial x$ and $\partial/\partial y$), which necessitates the collection of data in the horizontal direction, both streamwise and cross-stream.

We have also investigated the typically unexplored terms of the MKE budget equation. The MKE budget terms within the canopy indicate that the sum of the shear production term (which is the term through which the MKE and TKE interact with each other) and transport of turbulent fluxes by mean momentum is relatively inconsequential to the MKE tendency. Rather, it is the sinking of air under gravitational acceleration or the rising of air due to buoyancy that accounts for most of the variability in the MKE tendency (Figs. 9 and 10). This also indicates that the mean vertical velocity responds to the presence of a fire and cannot be assumed to be the same as the pre-FFP mean vertical velocity.

6. Conclusions and future work

Studies on turbulence during management-scale experimental burns conducted in differing conditions of wind and vegetation are relatively isolated. The integrated contextual framework provided in this work represents a major stride towards the synthesis of and comparison

among such studies. Through the comparison, we have reinvestigated fire-induced turbulence dynamics with the backdrop of canopy turbulence (forested environments) or ABL turbulence (grassland environment) from a fundamental standpoint. The effects of changes in ambient wind conditions on the measured data have been taken into account because of their linkage to fire behavior. While the inferences drawn here have also been informed by local meteorological conditions at the time of the burn experiments, we have successfully encapsulated the coherent patterns that broadly characterize fire-induced turbulent flow in the two environments primarily by examining turbulent fluxes and the TKE budget terms. We have also examined the terms of the MKE budget equation for all of the sub-canopy surface fire experiments. The sinking of air under gravitational acceleration or the rising of air due to buoyant updrafts accounts for most of the variability in the MKE tendency during and after fire-front passage. The "slowly-varying" mean flow responds noticeably to the presence of the fire and cannot be equated to the pre-FFP mean flow.

In this study, major differences among three scenarios of surface fires have been highlighted: sub-canopy heading fires, sub-canopy backing fires, and heading grassland fires. Differences in the relative strength and role of the streamwise and cross-stream turbulent eddies in fire spread and the relative importance of some terms of the TKE budget over others at each of the measurement heights have been discussed, based on fire intensity and the surface-fire environment. Shear production and buoyancy production in sub-canopy surface fires are found to be more substantial near the canopy top for more intense
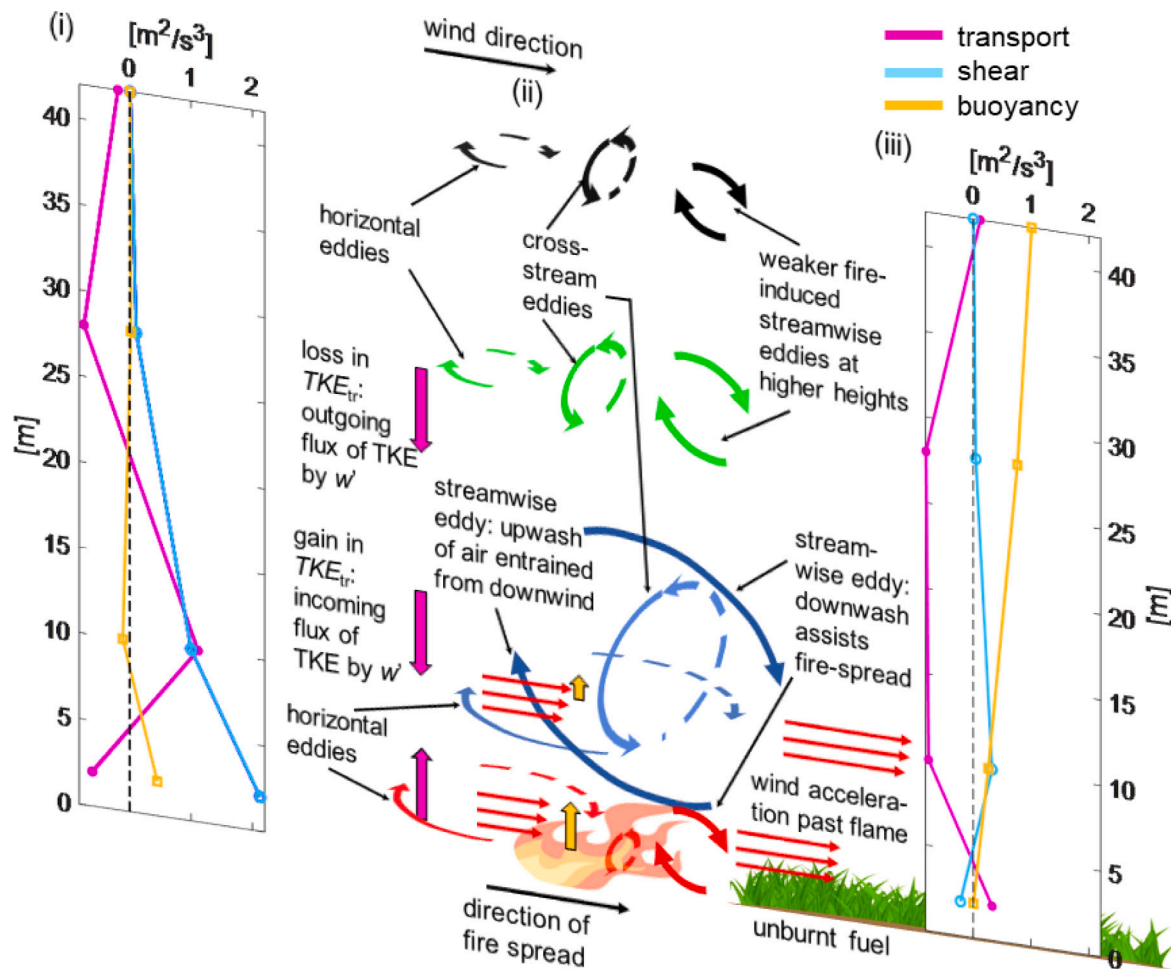
Fig. 11. A brief summary of the turbulent processes in the 2006 grassland fire (TX2006) along with profiles of the TKE budget equation terms for a time instant in the (i) FFP period and (iii) pre-FFP period. Note that post-FFP profiles are not shown here. Arrows are not to scale. (Vector figures of the green grass and the flame taken from *www.vecteezy.com/free-vector/grass* and *www.vecteezy.com/free-vector/flame*, respectively).

fires, while their magnitudes decrease with decreasing fire intensity. For low-intensity sub-canopy fires, the buoyancy production is considerably lower than the shear production near the canopy top, though the latter is mostly attributed to the background canopy turbulence. In a heading grassland fire, shear production dominates buoyancy production close to the surface and appears to be inconsequential beyond a certain height relative to the flame length, while buoyancy production increases with height thereby becoming substantial further away from the surface. In all sub-canopy fires, buoyancy production seems to dominate shear production at the mid-canopy height. The turbulent transport term appears to follow a coherent pattern during fire-front passage when the fire intensity is higher, both within the canopy and in a grassland environment. For intense sub-canopy surface fires, a noticeable loss in TKE due to its expulsion to the atmospheric boundary layer aloft via the transport term is compensated by a gain due to TKE influx via the transport term. In the grassland fire, the transport term shows similar behavior until a certain height. These differences also inform the vertical length scales associated with fire-induced turbulent flow in their respective environments. While such length scales have been quantified and studied in no-fire conditions in previous studies (Raupach et al., 1996), this study takes a step in the direction of quantifying length scales in the presence of a fire, which can inform smoke dispersion in different environments. The system of equations that governs fire dynamics is very complex. Model developers can utilize the knowledge of relatively important or less important terms associated with each height (relative to the vertical

length scale) to simplify their models or adjust their model complexity depending on the vegetative environment. This will lead to decreased model computational costs without loss of physical understanding. In conjunction with simplified models, the turbulence dynamics presented in this study can also be applied towards understanding the physics of ember transport (Koo et al., 2010; Fernandez-Pello, 2017; Thurston et al., 2017; Thomas et al., 2020) and estimating the horizontal distance covered by embers lofted by the fire plume before they land to generate spot fires.

Another step in the direction of simplifying the governing equations would involve parameterizing fire-atmosphere interactions via a modified flux-gradient approach (K theory). The authors plan on using this data to obtain better estimates of the eddy diffusivity in the presence of a fire that will account for the non-local turbulence in the canopy and the coupling between shear and buoyancy. Furthermore, it must be noted that there are limitations associated with the averaging scheme used for examining coherent motions: a larger averaging window delocalizes the coherent motions in time, while a smaller window makes it difficult to separate the mean terms from the turbulent fluctuations. The findings of this study could be augmented by inferences drawn from a wavelet transform on the temperature and velocity signals, which the authors are currently working on. With the help of a suitable window in the time domain, a wavelet transform could disassemble the signal into its component frequencies while achieving the best localization in time, thereby providing insights into the corresponding coherent motions and their temporal evolution.

Funding acknowledgment

CRediT authorship contribution statement

Ajinkya Desai: Writing – original draft, Writing – review and editing, Analysis-coding and interpretation. **Warren E. Heilman:** Writing – review and editing, Experimental data acquisition. **Nicholas S. Skowronski:** Writing – review and editing, Experimental data acquisition. **Kenneth L. Clark:** Writing – review and editing, Experimental data acquisition. **Michael R. Gallagher:** Writing – review and editing, Experimental data acquisition. **Craig B. Clements:** Writing – review and editing. **Tirtha Banerjee:** Analysis – supervision.

Declaration of competing interest

The authors declare that they have no known competing financial interests or personal relationships that could have appeared to influence the work reported in this paper.

Data availability

Data utilized by this study are available in the Forest Service Research Data Archive and can be accessed through the following links: http://dx.doi.org/10.2737/RDS-2017-0060, http://dx.doi.org/10.2737/RDS-2017-0062, http://dx.doi.org/10.2737/RDS-2022-0089, http://dx.doi.org/10.2737/RDS-2022-0090, http://dx.doi.org/10.2737/RDS-2022-0095. The FireFlux dataset can be requested through the following link: https://www.fireweather.org/data-request.

Appendix A. Supplementary data

Supplementary material related to this article can be found online at https://doi.org/10.1016/j.agrformet.2023.109501.

References

Andrews, P.L., 2014. Current status and future needs of the BehavePlus fire modeling system. Int. J. Wildland Fire 23 (1), 21–33.

Banerjee, T., 2020. Impacts of forest thinning on wildland fire behavior. Forests 11 (9), 918.

Clark, K., 2016a. AmeriFLUX US-CEd Cedar Bridge. tech. rep, Lawrence Berkeley National Lab. (LBNL), Berkeley, CA, United States.

Clark, K., 2016b. AmeriFLUX US-SLt Silas Little-NEw Jersey. tech. rep, Lawrence Berkeley National Lab. (LBNL), Berkeley, CA, United States.

Clements, C.B., Zhong, S., Bian, X., Heilman, W.E., Byun, D.W., 2008. First observations of turbulence generated by grass fires. J. Geophys. Res. Atmos. 113 (D22).

Clements, C.B., Zhong, S., Goodrick, S., Li, J., Potter, B.E., Bian, X., Heilman, W.E., Charney, J.J., Perna, R., Jang, M., et al., 2007. Observing the dynamics of wildland grass fires: FireFlux—A field validation experiment. Bull. Am. Meteorol. Soc. 88 (9), 1369–1382.

Colman, J.J., Linn, R.R., 2007. Separating combustion from pyrolysis in HI-GRAD/FIRETEC. Int. J. Wildland Fire 16 (4), 493–502.

Desai, A., Goodrick, S., Banerjee, T., 2022. Investigating the turbulent dynamics of small-scale surface fires. Sci. Rep. 12 (1).

Fernandez-Pello, A.C., 2017. Wildland fire spot ignition by sparks and firebrands. Fire Saf. J. 91, 2–10.

Finney, M.A., 1998. FARSITE, Fire Area Simulator–Model Development and Evaluation. (4), US Department of Agriculture, Forest Service, Rocky Mountain Research Station.

Finney, M.A., 2006. An overview of FlamMap fire modeling capabilities. In: Andrews, Patricia L., Butler, Bret W. (Eds.), Comps. 2006. Fuels Management-how to Measure Success: Conference Proceedings. 28–30 March 2006; Portland, OR. Proceedings RMRS-P-41, vol. 41. US Department of Agriculture, Forest Service, Rocky Mountain Research Station, Fort Collins, CO, pp. 213–220.

Finney, M.A., Cohen, J.D., Forthofer, J.M., McAllister, S.S., Gollner, M.J., Gorham, D.J., Saito, K., Akafuah, N.K., Adam, B.A., English, J.D., 2015. Role of buoyant flame dynamics in wildfire spread. Proc. Natl. Acad. Sci. 112 (32), 9833–9838.

Heilman, W.E., Banerjee, T., Clements, C.B., Clark, K.L., Zhong, S., Bian, X., 2021a. Observations of sweep–ejection dynamics for heat and momentum fluxes during wildland fires in forested and grassland environments. J. Appl. Meteorol. Climatol. 60 (2), 185–199.

Heilman, W.E., Bian, X., Clark, K.L., Skowronski, N.S., Hom, J.L., Gallagher, M.R., 2017. Atmospheric turbulence observations in the vicinity of surface fires in forested environments. J. Appl. Meteorol. Climatol. 56 (12), 3133–3150.

Heilman, W.E., Bian, X., Clark, K.L., Zhong, S., 2019. Observations of turbulent heat and momentum fluxes during wildland fires in forested environments. J. Appl. Meteorol. Climatol. 58 (4), 813–829.

Heilman, W.E., Clark, K.L., Bian, X., Charney, J.J., Zhong, S., Skowronski, N.S., Gallagher, M.R., Patterson, M., 2021b. Turbulent momentum flux behavior above a fire front in an open-canopied forest. Atmosphere 12 (8), 956.

Heilman, W.E., Clements, C.B., Seto, D., Bian, X., Clark, K.L., Skowronski, N.S., Hom, J.L., 2015. Observations of fire-induced turbulence regimes during low-intensity wildland fires in forested environments: implications for smoke dispersion. Atmos. Sci. Lett. 16 (4), 453–460.

Heilman, W.E., Zhong, S., Charney, J.J., et al., 2013. Development of modeling tools for predicting smoke dispersion from low-intensity fires. In: JFSP Research Project Reports.

Kiefer, M.T., Heilman, W.E., Zhong, S., Charney, J.J., Bian, X., 2015. Mean and turbulent flow downstream of a low-intensity fire: Influence of canopy and background atmospheric conditions. J. Appl. Meteorol. Climatol. 54 (1), 42–57.

Koo, E., Pagni, J., Weise, D.R., Woycheese, J.P., 2010. Firebrands and spotting ignition in large-scale fires. Int. J. Wildland Fire 19 (7), 818–843.

Lee, X., Massman, W., Law, B., 2004. Handbook of Micrometeorology: A Guide for Surface Flux Measurement and Analysis, vol. 29. Springer Science & Business Media.

Linn, R.R., Goodrick, S., Brambilla, S., Brown, M.J., Middleton, R.S., O'Brien, J.J., Hiers, J.K., 2020. QUIC-fire: A fast-running simulation tool for prescribed fire planning. Environ. Model. Softw. 125, 104616.

Linn, R., Reisner, J., Colman, J.J., Winterkamp, J., 2002. Studying wildfire behavior using FIRETEC. Int. J. Wildland Fire 11 (4), 233–246.

Mell, W., Jenkins, M.A., Gould, J., Cheney, P., 2007. A physics-based approach to modelling grassland fires. Int. J. Wildland Fire 16 (1), 1–22.

Morvan, D., Dupuy, J.-L., Rigolot, E., Valette, J.-C., 2006. FIRESTAR: a physically based model to study wildfire behaviour. Forest Ecol. Manag. (234), S114.

Mueller, E., Mell, W., Simeoni, A., 2014. Large eddy simulation of forest canopy flow for wildland fire modeling. Can. J. Forest Res. 44 (12), 1534–1544.

Pereira, D., 2022. Wind rose. https://www.mathworks.com/matlabcentral/fileexchange/47248-wind-rose. (Accessed 1 March 2022).

Raupach, M.R., Finnigan, J.J., Brunet, Y., 1996. Coherent eddies and turbulence in vegetation canopies: the mixing-layer analogy. In: Boundary-Layer Meteorology 25th Anniversary Volume, 1970–1995. Springer, pp. 351–382.

Rothermel, R.C., 1972. A mathematical model for predicting fire spread in wildland fuels. In: Intermountain Forest & Range Experiment Station, Forest Service, vol. 115. US Department of Agriculture.

Seto, D., Clements, C.B., Heilman, W.E., 2013. Turbulence spectra measured during fire front passage. Agricult. Forest. Meteorol. 169, 195–210.

Stull, R.B., 2012. An Introduction to Boundary Layer Meteorology, vol. 13. Springer Science & Business Media.

Sun, R., Krueger, S.K., Jenkins, M.A., Zulauf, M.A., Charney, J.J., 2009. The importance of fire–atmosphere coupling and boundary-layer turbulence to wildfire spread. Int. J. Wildland Fire 18 (1), 50–60.

Thomas, C., Sharples, J.J., Evans, J., 2020. The terminal-velocity assumption in simulations of long-range ember transport. Math. Comput. Simul. 175, 96–107.

Thurston, W., Kepert, J.D., Tory, K.J., Fawcett, R.J., 2017. The contribution of turbulent plume dynamics to long-range spotting. Int. J. Wildland Fire 26 (4), 317–330.

Tohidi, A., Gollner, M.J., Xiao, H., 2018. Fire whirls. Annu. Rev. Fluid Mech. 50, 187–213.

Zhou, X., Mahalingam, S., Weise, D., 2007. Experimental study and large eddy simulation of effect of terrain slope on marginal burning in shrub fuel beds. Proc. Combust. Inst. 31 (2), 2547–2555.